



**HAL**  
open science

# Episodic collisional orogenesis and lower crust exhumation during the Palaeoproterozoic Eburnean Orogeny: Evidence from the Sefwi Greenstone Belt, West African Craton

H.B. Mcfarlane, L. Ailleres, P. Betts, J. Ganne, L. Baratoux, M.W. Jessell, S. Block

## ► To cite this version:

H.B. Mcfarlane, L. Ailleres, P. Betts, J. Ganne, L. Baratoux, et al.. Episodic collisional orogenesis and lower crust exhumation during the Palaeoproterozoic Eburnean Orogeny: Evidence from the Sefwi Greenstone Belt, West African Craton. *Precambrian Research*, 2019, 325, pp.88 - 110. 10.1016/j.precamres.2019.02.012 . hal-03485917

**HAL Id: hal-03485917**

**<https://hal.science/hal-03485917>**

Submitted on 20 Dec 2021

**HAL** is a multi-disciplinary open access archive for the deposit and dissemination of scientific research documents, whether they are published or not. The documents may come from teaching and research institutions in France or abroad, or from public or private research centers.

L'archive ouverte pluridisciplinaire **HAL**, est destinée au dépôt et à la diffusion de documents scientifiques de niveau recherche, publiés ou non, émanant des établissements d'enseignement et de recherche français ou étrangers, des laboratoires publics ou privés.



Distributed under a Creative Commons Attribution - NonCommercial 4.0 International License

## **Episodic collisional orogenesis and lower crust exhumation during the Palaeoproterozoic Eburnean Orogeny: Evidence from the Sefwi Greenstone Belt, West African Craton**

McFarlane, H. B.<sup>1,2,3</sup>, Ailleres, L.<sup>1</sup>, Betts, P.<sup>1</sup>, Ganne, J.<sup>2</sup>, Baratoux, L.<sup>2,4</sup>, Jessell, M. W.<sup>3</sup>, Block, S.<sup>2</sup>

### Affiliations:

<sup>1</sup>School of Earth, Atmosphere and Environment, Monash University, 9 Rainforest Walk, Clayton, VIC 3800, Australia,

<sup>2</sup>GET, Observatoire Midi Pyrénées, IRD, 14 ave E. Belin, Toulouse 31400 France

<sup>3</sup>CET, The University of Western Australia, 35 Stirling Hwy, Crawley, WA 6009 Australia

[helen.mcfarlane@uwa.edu.au](mailto:helen.mcfarlane@uwa.edu.au) (*corresponding author - present address*)

<sup>4</sup> IFAN, Cheikh Anta Diop, Dakar, Senegal

## Abstract

New constraints on the architecture, deformation sequence and tectonic evolution of the sparsely exposed Palaeoproterozoic Sefwi Greenstone Belt (ca. 2200–2070 Ma) in SW Ghana are derived from the integration of field observations, structural mapping and interpretation of regional airborne geophysical data. Our findings provide new insights into the tectonic evolution of the West African Craton during the Palaeoproterozoic Eburnean Orogeny (ca. 2150–2070 Ma). Domains of contrasting metamorphic grade comprising high-grade paragneisses and meta-volcanic rocks are tectonically juxtaposed against low-grade volcano-sedimentary packages. The earliest deformation event is characterised by a bedding-parallel high-grade metamorphic foliation ( $S_1$ ) that is axial planar to isoclinal folds formed during NNW-SSE shortening and late- $D_1$  partial melting. This crustal thickening event generated biotite  $\pm$  muscovite granites emplaced parallel to the NW margin of the Sefwi Belt between ca. 2092 and 2081 Ma, providing a minimum age for  $D_1$ .  $D_2$  deformation is characterised by a moderate to steeply dipping, ENE-WSW to NE-SW striking, penetrative  $S_2$  mineral foliation. Within the Sefwi Belt, coaxial  $F_2$  fold axes and  $L_2$  stretching lineations pitch shallowly ENE-WSW to NE-SW, oblique to the major shear zones, indicative of ENE-WSW transtension and associated constrictional deformation. Differential exhumation of middle and lower crustal segments along NNE-striking  $D_2$  extensional detachments was coincident with sinistral oblique reactivation of NE-SW regional-scale shear zones. The timing of exhumation is constrained by metamorphic monazite U-Pb ages at ca. 2073 Ma. Subsequent E-W shortening is associated with dextral reactivation of regional NE-SW striking shear zones and refolding of earlier structures away from the major shear zones. We propose that the NW margin of the Sefwi Belt represents the collision ( $D_1$ ) of southern Ghana and central and NW Ghana/Ivory Coast which record different tectonic histories. Furthermore, we suggest the amalgamation of the West African Craton is the product of episodic collisional orogenesis, providing new insights into the evolution of orogenic processes during the Palaeoproterozoic.

**Keywords:** Palaeoproterozoic; collision; orogenesis; transtension; exhumation; West African Craton; Sefwi Greenstone Belt; Ghana

## 1. Introduction

The applicability of the plate tectonic paradigm when investigating accretionary and collisional orogenesis in the Precambrian is a continued source of controversy and debate (e.g. Cawood, *et al.*, 2006; Condie & Kröner, 2008; Fischer & Gerya, 2016; van Hunen & Moyen, 2012). Modern subduction-related convergent settings often comprise narrow fold and thrust belts, accretionary mélanges, ophiolites, blueschist facies rocks and ultra-high-pressure metamorphism (UHPM), many of which did not appear until the Neoproterozoic (Chopin, 2003; Ernst, 2005; Stern, 2005). In contrast, Archean and some Palaeoproterozoic geological provinces are characterised by granite-greenstone terranes, associated with high crustal growth rates (e.g. Dhuime, *et al.*, 2012), unique geochemical signatures and strain patterns (e.g. Bouhallier, *et al.*, 1995; Condie, 1994; de Wit, *et al.*, 1992; Keller & Schoene, 2012) and greenschist-to-granulite facies metamorphism (Harley, 1992; Komiyama, *et al.*, 2002). Each of these features reflect the influence of hotter ambient mantle temperatures early in the Earth's history (Herzberg, *et al.*, 2010; Korenaga, 2013). The ensuing dichotomous debate regarding early Earth tectonics has two primary end-members. The first suggests the granite-greenstone architecture is the product of gravitational instabilities and the downward advection, or sagduction, of cold, dense greenstone rocks and relative diapiric ascent of warm, buoyant felsic granitoids, known as *vertical tectonics* (Bouhallier, *et al.*, 1995; Choukroune, *et al.*, 1995; Van Kranendonk, *et al.*, 2007). In this model, associated lateral deformation is accommodated by bounding crustal-scale shear zones (Vidal, *et al.*, 2009). In the second alternate model, the shear zones are interpreted as major crustal sutures or thrust faults, juxtaposing contrasting litho-tectonic domains akin to modern accretionary-collisional orogens (e.g. Calvert, *et al.*, 1995; Feybesse, *et al.*, 2006; Polat & Kerrich, 1999).

Recently, a significant amount of research using numerical and thermo-mechanical modelling has focused on the influence of elevated mantle temperatures, and its subsequent secular cooling, on the viability of subduction, lithospheric rheology and the characteristics of orogenic processes in the early Earth (Ernst, 2009; Gerya, 2014; O'Neill, *et al.*, 2007; Rey & Houseman, 2006; Sizova, *et al.*, 2014; Sizova, *et al.*, 2010; Thébaud & Rey, 2013). In the rock record, such changes are reflected in the progressive diversification of preserved metamorphic conditions and the appearance of eclogite high-pressure granulite (EHPG) and ultra-high-temperature (UHT) facies rocks between ca. 3000 and 2000 Ma (e.g. Brown, 2006; 2007; Collins, *et al.*, 2004). EHPG facies metamorphism suggests a strengthening of the lithosphere and the commencement of subduction-like processes, whilst UHT metamorphism is attributed to the coupling of elevated geotherms in attenuated lithosphere and warmer mantle temperatures (e.g. Bhattacharya, 2004; Harley & Motoyoshi, 2000; Ouzegane, *et al.*, 2003).

Higher geotherms, elevated magmatism and crustal growth coincides with the development of collisional orogenesis in the Neoproterozoic and Palaeoproterozoic, prompting the invocation of a *hot-orogen* model for Precambrian accretionary orogens. These are characterised by monotonous HT-LP metamorphic condition, three-dimensional deformation and lateral flow during the compression of hot lithosphere (e.g. Cagnard, *et al.*, 2006; Vidal, *et al.*, 2009), attributed to the rheological weakening of new continental lithosphere by massive juvenile magmatism (Chardon, *et al.*, 2009, and references therein).

The Archean tectonic debate persists into the Palaeoproterozoic in the case of the granite-greenstone terranes of the West African Craton (2300–2070 Ma) (Abouchami, *et al.*, 1990; Boher, *et al.*, 1992). The formation and assemblage of this enigmatic juvenile cratonic domain coincides with the onset of nascent or episodic plate tectonics and ambient mantle temperatures approximately 100 – 200 °C greater than present day (Ganne & Feng, 2017; Herzberg, *et al.*, 2010). As for Archean terranes, authors have invoked gravitationally-driven vertical tectonics (e.g. Lompo, 2009; Vidal, *et al.*, 2009), subduction-related volcanic arc accretion (e.g. Baratoux, *et al.*, 2011; Feybesse, *et al.*, 2006) and collision (Block, *et al.*, 2016), as well as hot-orogen style deformation and metamorphism for the West African Craton (Chardon, *et al.*, 2009; Vidal, *et al.*, 2009). The Palaeoproterozoic rocks therefore represent a unique opportunity to explore orogenic processes during a transitional phase of the Earth’s history prior to the establishment of deep, self-sustaining subduction (Stern, 2007; Van der Hilst, *et al.*, 1997; van Hunen & van den Berg, 2008).

This paper focuses on the tectonic evolution of the Palaeoproterozoic crust of southwest Ghana, which comprises the Sefwi Greenstone Belt and the adjacent Sunyani-Comoé and Kumasi-Afema meta-sedimentary domains. Structural and metamorphic field observations are integrated with regional airborne geophysical data to interpret lithological and structural maps. The deformation sequence during the ca. 2100 Ma Eburnean Orogeny is constrained with existing geochronological data. This multi-scale, multi-discipline approach provides insight into the tectonic styles and exhumation mechanisms preserved within the craton. We discuss the implications of our findings relative to the Precambrian orogenic record and the secular evolution of metamorphism and thermodynamic properties of the lithosphere in the early Earth.

## **2. Geological Setting**

The southern portion of the West African Craton (WAC; Fig. 1a) comprises the Archean Kénéma-Man province (3600–2700 Ma), tectonically juxtaposed to the north and the east against juvenile granite-greenstone terranes of the Palaeoproterozoic (2300–1980 Ma) Baoulé-Mossi Domain

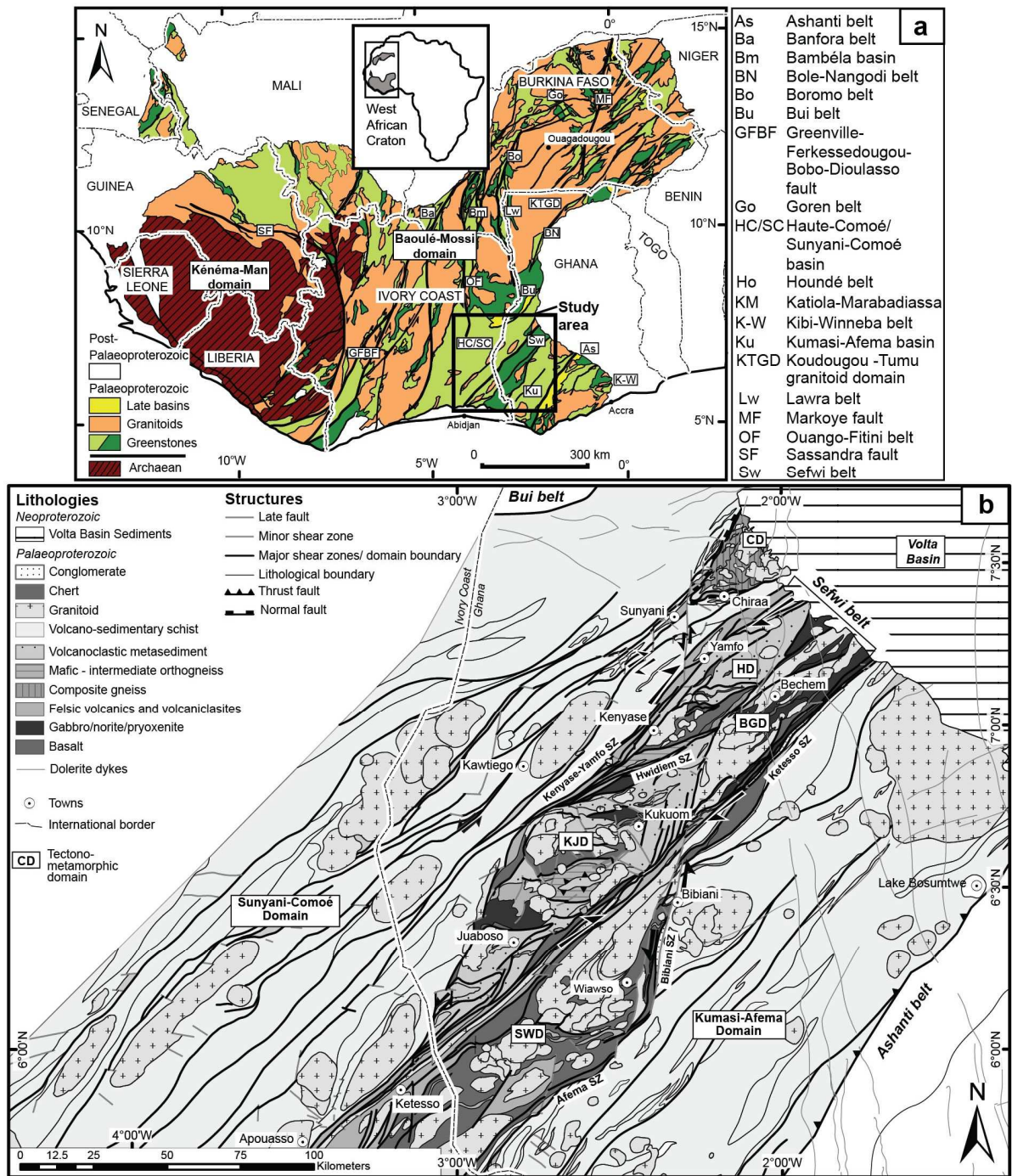


Fig. 1: a) The southern portion of the West African Craton showing the study area in the southeast, (modified after Milési, et al., 2004), with inset showing location of Archaean and Palaeoproterozoic domains of the West African Craton, Dark and light green colours represent mafic volcanic rocks and sedimentary rocks intercalated with intermediate to felsic volcanoclastite rocks, respectively. Yellow units comprise unconformably overlying fluvio-deltaic sediments in fault-bounded basins; b) Simplified map from this study showing dominant lithologies, domain names used within the text and major shear zones transecting the SW Ghana. CD: Chiraa Domain; HD: Hwidiem Domain; BGD: Bechem Granitoid Domain; KJD: Kukuom-Juaboso Domain; SWD: Sefwi-Wiawso Domain; SZ: Shear Zone.

(Bessoles, 1977; Rocci, 1965). Palaeoproterozoic formations are characterised by elongate volcanic-plutonic greenstone belts and volcano-sedimentary “basins” of the Birimian Supergroup, which are bounded by regional- to craton-scale shear zones (Junner, 1940; Leube, *et al.*, 1990) and often separated by voluminous granite-gneiss terranes. Birimian greenstone belts comprise basaltic to rhyolitic volcanic and volcanoclastite rocks displaying tholeiitic to calc-alkaline affinities (e.g. Baratoux, *et al.*, 2011; Dampare, *et al.*, 2008; Leube, *et al.*, 1990; Pouclet, *et al.*, 2006). Birimian basins consist of volcanoclastite, greywacke, argillite, shale and chemical sediments, intercalated with intermediate volcanic layers (e.g. Leube, *et al.*, 1990; Oberthür, *et al.*, 1998). The nature of the stratigraphic relationship between the two units are often ambiguous due to highly tectonised contacts.

A new stratigraphy for the Birimian Supergroup consisting of the Sefwi and Kumasi Groups was recently established in southern Ghana, based on rocks exposed in the Ashanti Belt and Kumasi Basin, by Adadey, *et al.* (2009) and Perrouty, *et al.* (2012). The Sefwi Group is defined as a formation of mafic to intermediate volcanic, volcanoclastite and subordinates sedimentary rocks emplaced between ca. 2195 and 2174 Ma (Perrouty, *et al.*, 2012, and referemces therein). Detrital zircon U-Pb and Pb-Pb data indicates that the deposition of volcano-sedimentary and sedimentary sequences of the younger Kumasi Group commenced after ca. 2150 Ma (Adadey, *et al.*, 2009; Davis, *et al.*, 1994; Oberthür, *et al.*, 1998). Sporadically and unconformably overlying central portions of many of the greenstone belts are fluvio-deltaic conglomerate, quartzite and phyllite sequences of the Tarkwa Group, in narrow, fault bounded basins (Davis, *et al.*, 1994; Eisenlohr, 1989). Detrital zircon U-Pb and Pb-Pb populations reveal a maximum age of deposition of  $2132 \pm 3$  Ma (Davis, *et al.*, 1994; Hirdes & Nunoo, 1994), or possibly as young as  $2090 \pm 17$  Ma (Pigois, *et al.*, 2003). Similar fluvial conglomerate and sandstone sequences of the Bui Belt, formerly referred to as Tarkwaian (Kiessling, 1997; Zitzmann, *et al.*, 1997), form the Banda Group and were deposited as syn-orogenic molasses sequences between ca. 2125 and 2120 Ma (de Kock, *et al.*, 2011; de Kock, *et al.*, 2012; Kiessling, 1997).

Granitoid emplacement in the WAC is considered to be partially contemporaneous with volcanism (e.g. de Kock, *et al.*, 2011; Feybesse, *et al.*, 2006; Gueye, *et al.*, 2008; Pawlig, *et al.*, 2006; Tshibubudze, *et al.*, 2013). Na-rich, calc-alkaline dioritic to granitic magmas and silicic, tonalite-trondhjemite-granodiorite (TTG)-like magmas yield crystallisation ages between ca. 2190 and 2130 Ma (Agyei Duodu, *et al.*, 2009; Doumbia, *et al.*, 1998; e.g. Gasquet, *et al.*, 2003; Hirdes, *et al.*, 1996; Tapsoba, *et al.*, 2013). Younger, more potassic granitoids and felsic lavas were emplaced between ~2130 and 2070 Ma in Senegal, Mali and along the Archaean-Palaeoproterozoic contact in the Ivory Coast, and in SW Ghana between ca. 2090 and 2080 Ma (e.g. Egal, *et al.*, 2002; Hirdes & Davis, 2002; Hirdes, *et al.*, 1992; Liégeois, *et al.*, 1991; Parra-Avila, *et al.*, 2017; Petersson, *et al.*, 2016).

The architecture, metamorphism and strain patterns of the Baoulé-Mossi Domain are attributed to the Palaeoproterozoic Eburnean Orogeny (Bonhomme, 1962) between ca. 2150 and 1980 Ma (Davis, et al., 1994; Oberthür, et al., 1998). Metamorphism of volcanic greenstone belts and volcano-sedimentary domains is largely restricted to lower- to upper greenschist facies (e.g. Béziat, *et al.*, 2000; Feybesse, et al., 2006; Kříbek, *et al.*, 2008; Mumin & Fleet, 1995) with amphibolite facies recorded within the contact aureole of plutons (e.g. Debat, *et al.*, 2003; Pons, *et al.*, 1995). These are juxtaposed with small windows of locally migmatitic, amphibolite-to-granulite facies orthogneisses and paragneisses sporadically exposed throughout the craton (Boher, et al., 1992; e.g. Caby, *et al.*, 2000; de Kock, et al., 2012; Lemoine, *et al.*, 1990; Opare-Addo, *et al.*, 1993). A number of recent studies, however, have reported regional medium-pressure, medium temperature (MP-MT) amphibolite facies metamorphism within greenstone belts of SW Ghana (Galipp, *et al.*, 2003; John, *et al.*, 1999), whilst areas of NW Ghana, Senegal and eastern Burkina Faso preserve early, relic high-pressure, low-temperature (HP-LT) assemblages (Block, *et al.*, 2015; Ganne, *et al.*, 2012; 2014), variably overprinted by amphibolite-to-granulite facies anatexis conditions. Results of these studies, and the documentation of high-pressure granulites along the Archean-Palaeoproterozoic tectonic contact (Pitra, *et al.*, 2010; Triboulet & Feybesse, 1998) suggest a greater diversity in metamorphic conditions than previously assumed.

The distribution and structural relationships of the granite-greenstone terranes, as well as high- and low-grade metamorphic domains, have drawn a number of interpretations regarding both the evolution of the Eburnean Orogeny and the tectonic style responsible for the present day architecture. Some authors propose a polyphase tectonic history involving the diachronous deformation and metamorphism of high- and low-grade terranes, with >2150 Ma old migmatitic gneissic crust interpreted as an older basement upon which the Birimian Supergroup was deposited (Boher, et al., 1992; Lemoine, et al., 1990). The event was variably termed the Tangaeen or Burkinian, however, it is now more widely referred to as the Eoeburnean, encompassing an earlier tectonic evolution between 2200 and 2150 Ma (de Kock, et al., 2012; Feybesse, et al., 2006; Hein, 2010; Tshibubudze, et al., 2013) and is followed by the Eburnean Orogeny *sensu stricto*. Alternatively, adjacent terranes with contrasting peak high-grade and low-grade conditions were interpreted to have undergone a concomitant evolution during monocyclic, progressive deformation (Block, et al., 2015; Block, et al., 2016; Eisenlohr & Hirdes, 1992; Galipp, et al., 2003; Gasquet, et al., 2003; Loh, *et al.*, 1999), and therefore represent different crustal depths that have been subsequently tectonically juxtaposed.

The mechanisms of burial and exhumation of high-grade terranes of the WAC are elucidated by several contrasting models. Deformation is attributed to either horizontal shortening of rheologically strong lithosphere accommodated by thrust faults and nappe stacking, akin to modern



orogens (Billa, *et al.*, 1999; Fabre, *et al.*, 1990; Feybesse, *et al.*, 2006; Milési, *et al.*, 1989; Milési, *et al.*, 1992). The exhumation of regional high-grade terranes exposed in NW Ghana is attributed to concurrent extensional gravitational collapse and contractional deformation acting on an overthickened lithosphere weakened by partial melting in the lower crust (Block, *et al.*, 2015; Block, *et al.*, 2016). Alternatively, some authors have invoked gravity-driven vertical movements of dense greenstone belts and buoyant granitoid domains, based on monotonous metamorphism, increasing only in granitoid contact aureoles, and interpreted dome and basin strain patterns (Pons, *et al.*, 1995; Vidal, *et al.*, 2009). In this model, exhumation of migmatitic rocks is interpreted as the product of buoyancy-driven ascent in a rheologically weak, hot orogenic crust, following homogeneous and distributed crustal thickening and extensive granitoid emplacement (e.g. Caby, *et al.*, 2000; Ganne, *et al.*, 2014; Pouclet, *et al.*, 1996; Vidal, *et al.*, 2009).

### **3. Study area**

#### *3.1 Litho-structural domains*

The NE-striking Sefwi-Greenstone Belt of southwest Ghana and southeast Ivory Coast comprises a diverse range of metamorphic rocks from greenschist facies to migmatitic packages, flanked to the northwest and southeast by low-grade meta-sedimentary rocks of the Sunyani-Comoé and Kumasi-Afema domains (Fig. 1b) (Agyei Duodu, *et al.*, 2009; Feybesse, *et al.*, 2006; Hirdes, *et al.*, 2007). Discrete domains are bounded and intersected by ENE-, NE- or ~N-striking shear zones.

##### *3.1.1 High-grade domains of the Sefwi Belt*

The Chiraa Domain (CD) is a triangular area in the northeast, reaching ~30 km in width, unconformably overlain to the east by Neoproterozoic sediments of the Volta Basin. It comprises highly heterogeneous lithological packages of paragneiss, rare granitic orthogneisses and hornblendites that are intruded by foliated two-mica granites and pegmatites, dated at ca. 2092 Ma (Agyei Duodu, *et al.*, 2009; Petersson, *et al.*, 2016). The paragneiss protoliths include greywacke, pelitic or volcanoclastite rocks that occur as elongate rafts that are occasionally migmatitic. Metamorphic assemblages and textures that indicate high-pressure amphibolite to granulite facies metamorphic conditions (McFarlane, 2018). The Chiraa Domain is flanked to the west and the south by low-grade metasedimentary units of the Sunyani-Comoé Domain, however the contact is not directly observed.

The Kukuom-Juaboso Domain (KJD) predominantly comprises poly-deformed upper-greenschist to amphibolite facies mafic to intermediate amphibolites and quartz-rich meta-greywackes

and metamorphosed volcano-sedimentary rocks and multiple generations of granodiorite, granite and mafic-ultramafic plutons. The ~150 km long domain is rhomboidal in shape and has a maximum width of 45 km. The Hwidiem Domain (HD) to the northeast is lithologically comparable but is separated by migmatitic mafic orthogneisses within the Hwidiem Shear Zone. Only two ages exist for the Kukuom-Juaboso Domain that constrain the timing of granodiorite emplacement at ca. 2135 Ma (Amponsah, 2012). The Bechem Granitoid Domain (BGD) is located in the south-eastern portion of the Sefwi Belt and contains weakly deformed granitoids with compositions varying significantly from quartz diorites to garnet-biotite granites and younger potassic biotite granites (Hirdes, *et al.*, 1993). Pyroxenite, gabbro and norite intrusions and high strain gneissic amphibolites are found proximal to the Ketesso Shear Zone, along which lies a greenschist facies meta-rhyolite flow dated at ca. 2189 Ma (Hirdes & Davis, 1998). Southeast of the rhyolite, strongly sheared conglomerates with abundant rounded quartzo-feldspathic lithics are observed along the tectonic contact between the Sefwi Belt and the Kumasi-Afema Domain and are regionally correlated with the Tarkwa Group (Agyei Duodu, *et al.*, 2009).

### *3.1.2 Low-grade domains of the Sefwi Belt*

The NE-SW-striking Sefwi-Wiawso volcano-plutonic domain (SWD), in the southern portion of the Sefwi Belt, extends for ~200 km from Bibiani in southwest Ghana into south-eastern Ivory Coast (Hirdes, *et al.*, 2007; Hirdes, *et al.*, 1993). The domain comprises greenschist facies tholeiitic to intermediate volcanic rocks with minor volcanoclastite and volcano-sedimentary sequences. Coeval volcanism and plutonism is dated between ca. 2180 and 2136 Ma, ranging in composition from quartz diorites and monzodiorites to biotite granites (Agyei Duodu, *et al.*, 2009; Hirdes, *et al.*, 1992; Hirdes, *et al.*, 2007). Immature, polymictic conglomerates, sourced from both the volcano-plutonic rocks and the adjacent low-grade metasedimentary domains (Hirdes, *et al.*, 1993), occur at the easternmost boundary of the domain bound by the Bibiani Shear Zone (Agyei Duodu, *et al.*, 2009).

### *3.1.3 Low-grade meta-sedimentary domains/basins*

The Kumasi-Afema and Sunyani-Comoé meta-sedimentary domains comprise deformed volcanoclastite rocks, wacke, shale and argillite and rare intercalated felsic volcanic layers (Hirdes, *et al.*, 1993). The minimum deposition ages, constrained by granodiorite and leucogranite intrusions, for both domains are  $2136 \pm 2$  Ma and  $2088 \pm 2$  Ma, respectively (Adadey, *et al.*, 2009; Hirdes, *et al.*, 1992). Along strike of the Sunyani-Comoé Domain intrusions, granite plutons within the Chiraa Domain yield comparable ages of ca. 2092 Ma (Agyei Duodu, *et al.*, 2009; Petersson, *et al.*, 2016).

### 3.2 Major Shear Zones

The NE-striking Sefwi Shear System defines the regional architecture and major crustal-scale structures that extend >300 km from central Ghana to southeast Ivory Coast (Jessell, *et al.*, 2012). The northwest margin of the belt comprises sub-vertical NE-striking and south-dipping shear zones of the Kenyase-Yamfo Shear Zone, truncating the ENE-striking Hwidiem Shear Zone, which lies within the Sefwi Belt. The central Ketesso Shear Zone transects the length of the Sefwi Belt, from central Ghana to south-east Ivory Coast. It separates the Sefwi-Wiawso and Kukuom-Juaboso domains, forming the southern extent of the Bechem Granitoid Domain (Hirdes, *et al.*, 2003; Jessell, *et al.*, 2012). The southern-most NE-striking Afema Shear Zone marks the SE-dipping tectonic contact between the Sefwi-Wiawso volcano-plutonic domain and the Kumasi-Afema meta-sedimentary domain.

## 4. Methodology and data

Our interpreted geological map integrates field mapping with interpretation of regional geophysical data sets. Outcrop is sparse, precluding continuous mapping, however, lithological, structural and petrophysical information was acquired at 484 outcrop localities. This data was complemented by outcrop maps and observations from Hirdes, *et al.* (1993), as well as outcrop databases from mining companies (Kinross and Newmont).

### 4.1 Processing and interpretation of geophysical data

The Ghanaian data is a composite grid of five individual surveys, the details and locations of which are shown in the supplementary information (Supplementary Material: Fig. 1SI and Table 1SI). Four surveys have line spacings of between 200 and 500m and flight altitudes of between 70 and 80 m. Data was collected along E-W flight lines. The national airborne magnetic data of Ivory Coast was collected along N-S flight lines with a line spacing of 500 m and a flight altitude of 152 m (Fig. 1SI). Raw data was processed using Geosoft Oasis Montaj software and used for regional interpretations. Processed images are shown as supplementary files (Fig. 2SI–4SI).

#### 4.1.1 Aeromagnetic data

Airborne magnetic surveys provide us with a map of magnetic anomalies from which we can derive lithological, structural and kinematic information, as constrained by field observations (Aitken & Betts, 2009; Betts, *et al.*, 2007; Lindsay, *et al.*, 2011; Stewart, *et al.*, 2009). The magnetic data was gridded as a composite residual magnetic intensity (RMI) grid with a cell size of 100 m (Ghana) and 125 m (Ivory Coast). Residual magnetic intensity datasets covering SW Ghana and the Ivory Coast and the

A1 total magnetic intensity (TMI) grid were reduced to the equator (RTE), with a 180-degree phase reversal or inversion (negative RTE) (Fig. 2a) according to the method of Luo *et al.* (2010). Given the equatorial latitudes, conventional reduction to the pole (RTP) was unstable (Li, 2008; MacLeod, *et al.*, 1993) (Fig. 1SI). Interpretation of lithology distribution relied on both the negative RTE and analytical signal grids (MacLeod, *et al.*, 1993). Filters included the first vertical derivative, tilt derivative and amplitude normalisation (Automatic Gain Control), which were used to delineate structural trends and lithological boundaries (Gunn, *et al.*, 1995; Milligan & Gunn, 1997; Pilkington & Keating, 2009; Verduzco, *et al.*, 2004).

#### 4.1.2 Radiometric (gamma-ray) data

Gamma-ray spectrometry data shows the content and distribution of radioactive elements in the rocks and regolith in the uppermost 30cm of the Earth's crust (Minty, *et al.*, 1997; Wilford, *et al.*, 1997). Combined use of topographic information and geochemical data highlights lithology distribution and laterite and regolith cover (Dickson & Scott, 1997; Wilford, *et al.*, 1997). U, Th, and K bands were gridded individually at 100 m resolution (Fig. 4SI). A ternary RBG (Red-Green-Blue) diagram was draped over a shaded image of the digital elevation model (90 m resolution; Shuttle Radar Topographic Mission, SRTM, 2000). Band ratio (U/K and Th/K) and Principal Component Analysis (PCA) images were derived from the original bands. Relative abundance ratios were used to distinguish changes in rock type and alteration.

#### 4.1.3 Gravimetric data

Gravimetric data was sourced from the International Gravimetric Bureau (<http://bgi.omp.obs-mip.fr/>) as EGM08 Free Air and Bouguer anomaly grids, with a grid size of 1 arc-minute. The Bouguer anomaly map (Fig. 2SI) shows long wavelength anomalies is most effective at differentiating regional rock domains, large lithological packages and the extent of major structures along strike.

## 5. Lithological associations and geological map

The geophysical datasets were integrated within a GIS software for interpretation, according to the method of Metelka, *et al.* (2011). Integration of field data, petrophysical data and geophysical signatures were used to characterise the principal lithological associations (Table 1) in the new litho-structural map (Fig. 2b), with field photographs presented in Fig. 6SI. Magnetic susceptibility values for each unit are presented in Supplementary Information (Fig. 5SI). Values for magnetic anomalies are derived from the negative RTE image colour bar legend, and, as a product of data processing, are given as negative integers.

## 5.1 Lithologies

### 5.1.1 Basalt/metabasalt/metadolerite

Greenschist to amphibolite facies metabasalts and metadolerites are variably deformed with foliation intensity varying depending on proximity to larger faults and shear zones. In the airborne magnetic surveys, these mafic volcanic rocks have high-amplitude, high-frequency magnetic anomalies. The anomalies are elongate and curvilinear, ranging between 10 and 40 km in length, with variable amplitudes between -618 to -509 nT and -816 to -745 nT, consistent with multi-modal magnetic susceptibility values from 0.05 to  $84 \times 10^{-3}$  SI. Magnetic anomalies distal to major shear zones are parallel with the  $S_1$  foliation suggesting the magnetic data is imaging the earliest foliation. The dark radiometric signal of basalts indicates depletion in incompatible elements, however, units located along shear zones or domain boundaries show evidence of potassic alteration.

### 5.1.2 Meta-andesite/dacite

Andesitic and dacitic rocks occur within the Kukuom-Juaboso and Sefwi-Wiawso domains, as well as rare intercalated sills in the adjacent metasedimentary domains. Andesitic lavas are characterised by homogeneous to slightly stippled, low to moderate amplitude magnetic response. They are consistently lower amplitude (-710 to -620 nT) and often have longer magnetic wavelengths compared with the metabasalts. Andesitic layers have a bimodal magnetic susceptibility of  $0.03\text{--}0.40 \times 10^{-3}$  SI and  $7.41\text{--}39.50 \times 10^{-3}$  SI. The units are often associated with distinct eU enrichment relative to eTh and K in the radiometric data.

### 5.1.3 Rhyolite/felsic volcanoclastite/meta-rhyolite

Rhyolites, felsic volcanoclastites and pyroclastic units are found as narrow layers, parallel to stratigraphic layering in schists derived from volcano-sedimentary rocks in the Sunyani-Comoé and Kumasi-Afema domains. These felsic lava flows and volcanoclastites have discrete, elongate bimodal, high- and low- amplitude magnetic anomalies (-783 to -750 nT; -618 to -585 nT), parallel to observed bedding. Magnetic susceptibilities are generally low ( $< 0.60 \times 10^{-3}$  SI), however, more magnetite-rich felsic volcanoclastic layers yield magnetic susceptibility values of  $6.25\text{--}29.14 \times 10^{-3}$  SI. Their radiometric signal reveals high K and eTh content relative to eU.

Table 1. Synthesis of the mineralogy, petrophysical properties and geophysical signatures of the lithologies represented on the geological map (Fig. 2). Thumbnails represent subsets of geophysical datasets, each with 4km scale-bar, using the same methodology as described in section 4. Scale bar is 4km in length.

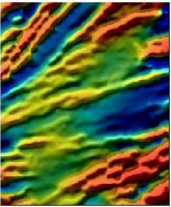
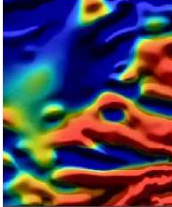
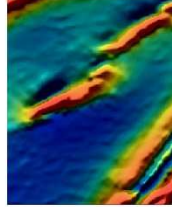
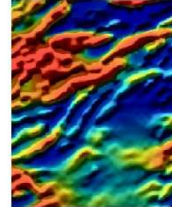
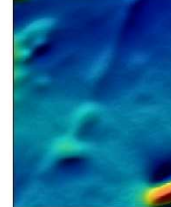
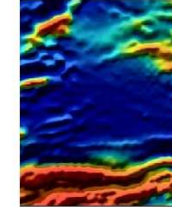
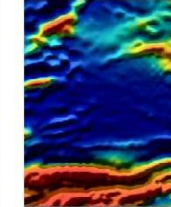
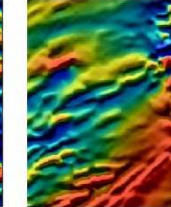
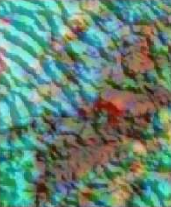
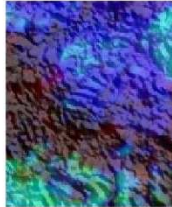

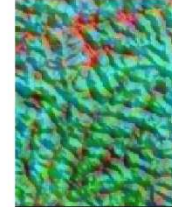



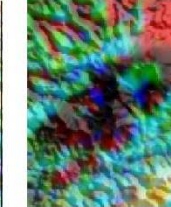

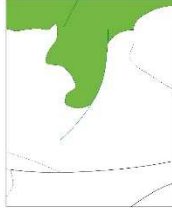
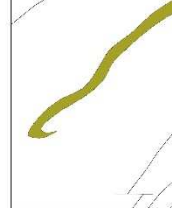

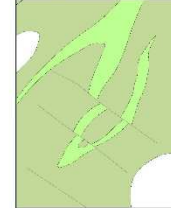

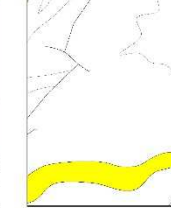

Lithology	Basalt/metabasalt/ metadolerite	Meta-andesite/dacite	Rhyolite/felsic volcaniclasite	Volcaniclastic metasediments	Volcano- sedimentary schist	Composite gneiss	Mafic orthogneiss	Gabbro/norite/pyrox enite complex
Mineralogy	Hbl, qz, (relict Cpx), bt, pl, chl, act,	pl, hbl, qz, ep, ttn, chl, act	qz, chl, wm, 29.14	Qz, pl, chl, wm, ± bt, hbl, grt	qz, chl, ms, gr	qz, bt, pl, wm, grt, ± alsi, tur, gr	pl, hbl, qz, ilm, grt, ep, ttn	hbl (after cpx), pl, chl, ep, act
Magnetic susceptibility rangc (10 <sup>-3</sup> SI)	0.05, 1.01 9.58, 13.08 84.00 (multimodal)	0.03 0.40, 7.41 39.50 (bimodal)	0.02 1.60, 6.25 29.14 (bimodal)	0.06 1.00, 20.01 80.30 (bimodal)	0.02 1.30	0.04 1.30	0.12 9.58 (bimodal)	0.27 2.48
Sample	SB040	SB173	SB044	SB439	SB362	SB398	SB177	SB411
U (ppm)	0.90	1.70	1.50	1.60	1.40	1.50	0.40	0.80
Th (ppm)	1.80	4.60	6.30	3.70	4.10	4.60	0.20	1.60
K <sub>2</sub> O (wt%)	1.17	1.54	2.3	2.63	2.79	3.16	0.2	0.81
Airborne magnetic response	Highly magnetic Heterogeneous, elongate near SZ	Low to high intensity	Low to very highly magnetic layers	Low to high, heterogeneous, strong mag. fabric	Low intensity, uniform, smooth	Very low to low intensity, smooth	Low to high intensity, variable	Low to moderate intensity, weak magnetic fabric
Magnetic image								
Airborne radiometric response	U, Th, K poor (dark), pervasive K alteration along SZ	Enriched in U relative to Th and K	Low U, moderate Th, high K (red - orange)	Low U, K, moderate Th, regolith (light blue)	Low U, Th, mod K, higher K in Kumasi domain (pink - red)	Moderate to high U, Th, K (pink-yellow)	Heterogeneous signal often covered by regolith and	U, Th, K poor (dark)
Radiometric response + shaded DEM								
Map								

Table 1. (continued)

Lithology	G1: Trondhjemite, tonalite, granodiorite	G2: Trondhjemite and granodiorite	G3a: Granodiorite, quartz diorite	G3b: Potassic quartz monzonite	G4: Leucogranite	Chemical sediment (Chert)	Polymictic conglomerate	Dolerite dyke
Mineralogy	qz, pl, bt, hbl, ± kfs	qz, pl, bt, hbl, ± kfs, ep	pl, kfs, qz, hbl, bt,	qz, kfs, pl, bt (± hbl)	qz, kfs, pl, bt, ms,	No data	qz, pl, chl, wm, ep, py	ol, opx, cpx, pl, hbl, bt
Magnetic susceptibility range ( $10^{-3}$ SI)	0.15 0.55, 1.01 3.50, 15.47 25.30 (multimodal)	0.12 2.03	0.09 1.00, 4.25 - 24.04 (bimodal)	0.47 3.88	0.00 0.15	0.35 1.59	0.01 0.50	0.08 0.16, 10.55 87.70 (bimodal)
Sample	SB252	SB248	SB045	SB023	SB010	SB171	SB417	SB431
U (ppm)	1.90	0.50	2.00	0.60	7.20	no data	no data	0.89
Th (ppm)	4.70	1.50	5.70	0.50	4.20			2.91
K <sub>2</sub> O (wt%)	1.84	1.24	1.82	4.01	2.51			1.13
Airborne magnetic response	Low to moderate intensity, strong magnetic fabric	Low to moderate, homogeneous, smooth	Moderate magnetic intensity, weak magnetic fabric	Moderate to high, moderate strength magnetic fabric	Low, homogeneous	Variable low to moderate intensity	Narrow, low intensity signal	Strong, linear signal
Magnetic image								
Airborne radiometric response	K, Th, U poor (dark) heterogeneous	Heterog. relative enrichment in Th; U, K poor (dark)	Low K, high Th, low U (green)	High K, mod U, low Th (red - pink)	High K, moderate Th, U,	Depleted in U, Th and K (dark)	High in K, U, Th (white) and rich in K close to SZ	No clear signal
Radiometric + shaded DEM								
Map								

#### 5.1.4 *Volcanoclastite rocks*

Immature, volcanoclastite and pyroclastic rocks with subordinate epiclastic meta-greywacke units and rare iron-rich quartzites occur in the Kukuom-Juaboso and Hwidiem domains. These rocks are metamorphosed at upper greenschist to amphibolite facies conditions. Biotite ± amphibole and garnet schistose to gneissic foliations alternate with quartz and plagioclase bands. The magnetic response of volcanoclastite rocks indicate heterogeneous magnetite distribution with alternating highly magnetic and non-magnetic layers. Magnetic amplitudes vary from -585 to -509 nT and -816 to -760 nT, with short, high-frequency wavelengths. The strong magnetic fabric shows excellent correlation with  $S_1$  foliations and is therefore used to extrapolate  $S_1$  trajectories. The magnetic susceptibility of this rock was bimodal, with values ranges from low ( $< 1 \times 10^{-3}$  SI) to extremely high (20.01–80.30  $\times 10^{-3}$  SI). The radiometric signal indicates Th enrichment relative to U and K, commonly masked by regolith cover, indicating extensive weathering.

#### 5.1.5 *Volcano-sedimentary schist*

The volcano-sedimentary schist unit is found mainly within the Sunyani-Comoé and Kumasi-Afema domains and comprises argillitic schist, graphitic shale, greywacke and minor intercalated felsic to intermediate volcanic rocks metamorphosed under sub-greenschist to greenschist facies conditions indicated by variably pervasive chlorite-white mica and chlorite-actinolite schistosity. Elevated metamorphic grade of the schistose units is limited to narrow contact aureoles of intruding granitoids. The aeromagnetic response of the metasedimentary rocks from the Kumasi-Afema Domain is a smooth low wavelength, with low- to moderate amplitudes (-690 to -605 nT). Higher amplitude magnetic responses and dipole magnetic anomalies are associated with shear zones. The volcano-sedimentary schists and intermediate volcanic rocks in the Sunyani Comoé Domain are characterised by a prominent bimodal magnetic signal. A smooth, wide and elongate, low-amplitude signal (-816 to -684 nT) occurs immediately north of Kenyase and to the north of Sunyani. Volcano-sedimentary schists along strike of intruding leucogranites often have a high magnetic response characterised by strong ENE-striking magnetic fabrics with high amplitude (-620 to -545 nT) and high frequency, which we attribute to the production of magnetite during prograde metamorphic reactions in granitoid aureoles, coupled with structurally controlled fluid flow. Magnetic susceptibility values are low (0.02–1.30  $\times 10^{-3}$  SI). The radiometric signal reveals K and eTh enrichment relative to eU in the Kumasi-Afema Domain and indicates extensive regolith cover in the Sunyani-Comoé Domain.



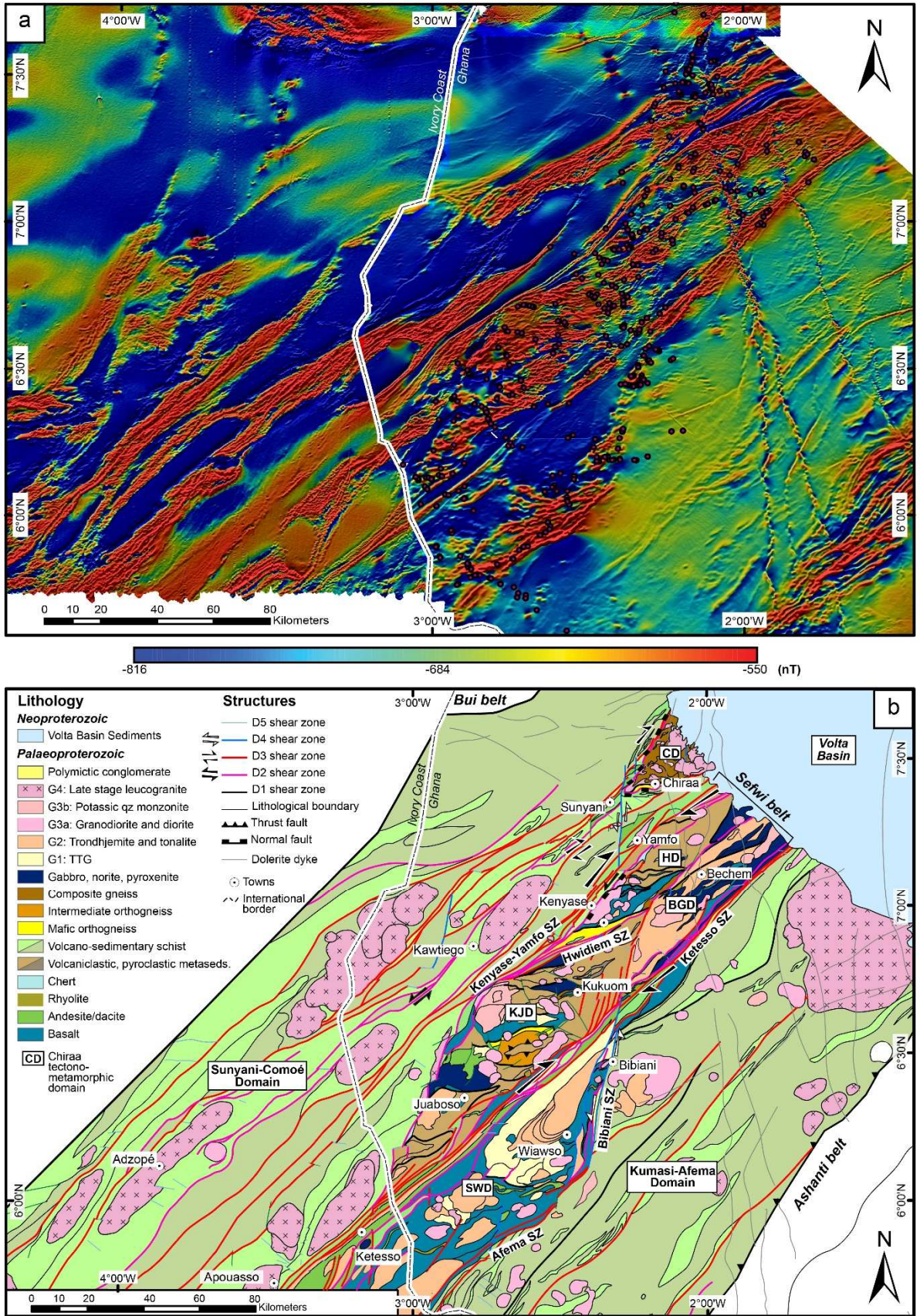


Fig. 2: a) Composite image of the negative reduced to the equator (nRTE) residual magnetic intensity draped over the shaded first vertical derivative (IVD), comprising airborne magnetic surveys from SW Ghana and SW Ivory

Coast (survey details in Fig. A1SI), displaying all outcrop localities; b) Lithological and structural map of the Palaeoproterozoic rocks of SW Ghana. CD: Chiraa Domain; HD: Hwidiem Domain; BGD: Bechem Granitoid Domain; SWD: Sefwi-Wiawso Domain; SZ: Shear Zone. Shear zones are colour coded according to the last deformation event during which they were active. Darker colours of the same lithological unit represent more rocks with a higher magnetic response.

#### 5.1.6 Composite gneiss

This package occurs in the Chiraa Domain and comprises paragneisses, rare granitic orthogneisses, varying proportions granitic and trondhjemitic melts and pegmatite dykes. A bedding parallel foliation in the paragneiss units is defined by biotite-rich and quartz-plagioclase-rich bands. A weak biotite foliation occurs in some granites. The composite gneiss, comprising both paragneisses and orthogneisses, has a low-amplitude (-816 to -765 nT), long wavelength aeromagnetic response with a weak magnetic fabric that is truncated by linear anomalies associated with younger faults. Minor proportions of the domain are characterised by a short wavelength, higher magnetic signal (-618 to -550 nT) defining a stronger magnetic horizons, possibly indicating heterogeneous magnetite concentration in stratigraphic layers. Magnetic susceptibility values of paragneisses and granites are predominantly low ( $0.04\text{--}1.30 \times 10^{-3}$  SI). The radiometric signal indicates moderate eU, eTh and K enrichment.

#### 5.1.7 Mafic orthogneiss

Mafic orthogneisses are exposed along the Hwidiem Shear Zone (Fig. 1b) and the southern margin of the Chiraa Domain. A migmatitic mafic orthogneiss in the Chiraa Domain has garnet and clinopyroxene porphyroblasts with plagioclase-rich leucosomes indicating high-pressure amphibolite–granulite facies conditions (Pattison, 2003). The magnetic response of the mafic orthogneiss is generally characterised by high-amplitude (-585 to -509 nT), elongated anomalies, subparallel to D<sub>1</sub> and D<sub>2</sub> shear zones. Occasional lower amplitude responses below -750 nT are associated with migmatitic mafic orthogneisses containing high melt proportions (e.g. western segment of the Hwidiem Shear Zone). Magnetic susceptibilities of mafic orthogneiss ranges from 0.12 to  $9.58 \times 10^{-3}$  SI.

#### 5.1.8 Gabbro-pyroxenite-norite

This package is a variably deformed hornblende-bearing gabbro, norite and clinopyroxene-rich pyroxenite, and layered hornblende-bearing mafic and dioritic intrusive suites. These lithologies are limited to the Kukuom-Juaboso, Bechem and Hwidiem domains in the central Sefwi Belt. They have a highly irregular magnetic texture with low frequency, low amplitude (-784 to -683 nT) anomalies

with weakly magnetised horizons that increase in magnetisation along faulted margins. They are characterised by low to moderate magnetic susceptibility ( $0.27\text{--}2.48 \times 10^{-3}$  SI) and gamma ray emissions indicate a strong depletion in incompatible elements. Where more strongly deformed, the radiometric signal indicates high eU and eTh relative to K, caused by the extensive lateritic or regolith cover (Dickson & Scott, 1997). This intrusive complex has not been directly dated.

#### *5.1.9 Granitoids*

Several suites of granitoids are identified. Trondhjemite, tonalite and rare granodiorite plutons (G1) contain biotite as the main ferromagnesian phase, with minor amphibole. They are foliated and locally migmatitic. K-feldspar is present in (micro) granodiorite plutons. The G1 suite has a low amplitude (-810 to -706 nT), moderate frequency, stippled textured aeromagnetic response. Magnetic susceptibility is multi-modal, ranging from  $0.15\text{--}25.30 \times 10^{-3}$  SI. Gamma-ray emissions indicate a heterogeneous depletion in radioactive elements.

A second group of granitoids comprise biotite-bearing, foliated to gneissic trondhjemite and tonalite plutons, with subordinate to rare amphibole (G2). The G2 granitoids are rounded to elongate and have a smooth, low to moderate (-783 to -684 nT) magnetic response. Magnetic susceptibility values ranging from  $0.12 - 1.03 \times 10^{-3}$  SI. The relative chronology of G1 and G2 suites is deduced from crosscutting relationships gleaned from aeromagnetic data stippled magnetic anomalies of the G1 suite, which are truncated by the smooth, long wavelength, low amplitude responses of the G2 suite. Gamma-ray emissions indicate an overall depletion in radioactive elements and relative enrichment in eTh. The 50km long Tano River trondhjemitic batholith, located immediately north of Wiawso, is associated with a large low response in the gravity data.

A third group of small, irregular bodies comprises calc-alkaline, coarse-grained, equigranular amphibole-bearing granodiorites and quartz diorites (G3a). The magnetic signal is sub-elliptical in shape with a heterogeneous, high frequency, low to high amplitude (-717 to -651 nT) magnetic response. Their radiometric signal indicates heterogeneous eTh enrichment relative to eU and K, with other areas indicating depletion in all incompatible elements. The magnetic susceptibility of these granitoids is bimodal, with values ranging from low ( $< 1 \times 10^{-3}$  SI), to locally highly magnetic ( $4.25 - 24.04 \times 10^{-3}$  SI).

Porphyritic potassic quartz monzonite plutons with abundant biotite and K-feldspar (G3b) are characterised as elliptical, sometimes, slightly elongate, with a distinct radiometric signal indicating enrichment in K relative to eTh and eU, strongly contrasting the radiometric signal of G3a. The aeromagnetic response of G3b granitoids is distinguished due to its moderate amplitude (-637 to -600

nT) and a more stippled texture, suggesting a heterogeneous distribution of magnetite. The G3b suite magnetic susceptibility values are low to moderate ( $0.47\text{--}3.88 \times 10^{-3}$  SI) and display a weak to well-defined magnetic fabric in airborne magnetic data.

Muscovite and biotite bearing leucogranites associated with coarse-grained, muscovite-rich pegmatitic bodies (G4) are identified from the aeromagnetic data as elongate ( $\sim 30\text{--}40$  km), elliptical plutons parallel to the NW-striking tectonic contact between the Sefwi Belt and the Sunyani-Comoé Domain. The magnetic response of the G4 suite is characterised by smooth, low amplitude ( $-816$  to  $-750$  nT), and long wavelength ( $>10$  km) magnetic responses. Their magnetic susceptibility values are homogeneously low ( $< 0.15 \times 10^{-3}$  SI). The radiometric signal for the G4 suite indicates enrichment in K and eTh, relative to eU. Gamma-ray emissions of large pegmatite bodies indicate enrichment in all incompatible elements. These bodies share similar petrological and petrophysical characteristics to ME3 of Baratoux, et al. (2011) and Metelka, et al. (2011) and G5 of Block, et al. (2016).

#### *5.1.10 Chemical sediment (Chert)*

Chemical sedimentary rocks are composed of massive or banded chert, located along the north-western and far western margins of the Kukuom-Juaboso and Hwidiem domains. Chert is characterised by an asymmetrical, elongate ( $\sim 5$  km), low amplitude ( $-783$  to  $-771$  nT), irregular aeromagnetic anomalies. Magnetic susceptibility values are generally low ( $0.35\text{--}1.59 \times 10^{-3}$  SI) and the radiometric signal indicates a depletion in all incompatible elements.

#### *5.1.11 Polymictic conglomerate and sandstone*

Two types of polymictic conglomerate and sandstone units are confined to the Ketesso Shear Zone and the Bibiani Shear Zone. Along the Ketesso Shear Zone, this lithology comprises strongly sheared sandstone, siltstone and matrix supported conglomeratic beds with intensely sheared, rounded quartzofeldspathic clasts. Conglomerates located along the Bibiani Shear Zone contain metasedimentary schist, meta-volcanic and granite-derived lithics, indicating local sources. A steeply dipping S-C fabric with a horizontal mineral stretching lineation is defined by quartz-chlorite-white mica or quartz-chlorite-actinolite metamorphic assemblages. This lithology is associated with narrow, elongate heterogeneous magnetic anomalies and has a radiometric signal that indicates high K and eTh.

#### *5.1.12 Volta basin sediments*

The Neoproterozoic Volta Basin sediments unconformably overlie the Palaeoproterozoic units in the NE. The sediments comprise horizontal beds of thick cross-bedded sandstone, fine-grained arkoses and rare conglomerates (Junner, 1946; Kalsbeek, et al., 2008). The basin is magnetically transparent.

The basin margin is most clearly defined in the combined DEM and radiometric image, associated with an elevated topography and extensive K depletion relative to eU and eTh.

#### *5.1.13 Dolerite dykes*

Dolerite dykes are characterised by high-amplitude (-509 nT), linear magnetic anomalies, several tens of metres wide and 40 to 200 km long. The dykes crosscut all Palaeoproterozoic formations with three primary orientations at N 340°, N 020° and N 070°. The dipole response characterising some dykes indicates strong magnetic susceptibility and remanence. Most intrudes the overlying Neoproterozoic Volta basin successions in the northeast of the field area.

#### *5.2 Geophysical response of tectono-metamorphic domains*

We identify several distinct tectono-metamorphic domains based on their geology, metamorphic grade and geophysical response. Domain boundaries are defined by magnetic linear anomalies, truncation of magnetic fabrics or contrasting magnetic, radiometric or gravity responses. Tectono-metamorphic domains within the Sefwi Belt, including the high-grade Chiraa Domain, correspond with a NE-striking, high amplitude gravity anomaly (Fig. 2SI). Moderate to low gravity responses flank the belt to the northwest and southeast, corresponding with meta-sedimentary units of Sunyani-Comoé and Kumasi-Afema Domains, respectively. The aeromagnetic data yields more detail on the lithology distribution and domain boundaries within the Sefwi Belt (Fig. 2a).

The central, Kukuom-Juaboso and Hwidiem domains are characterised by a strong, E-W to ENE-WSW trending magnetic fabric (Fig. 2a, b), predominantly associated with metamorphosed volcanoclastite and greywacke sequences. Magnetic fabrics of the Kukuom-Juaboso Domain are truncated to the west and to the east along NNE-striking structures, interpreted as the domain boundaries. The bounding Kenyase-Yamfo and Hwidiem shear zones are defined by elongate, narrow, NE- and ENE-striking magnetic lineaments respectively. In contrast, the Chiraa Domain is characterised predominantly by a low magnetic signal containing discrete, high magnetic anomalies, consistent with the heterogeneous high-grade paragneiss and granite exposures within the domain. The Bechem Granitoid domain is characterised by a low- to moderate magnetic response, with a weak, heterogeneous magnetic fabric, with high amplitude, linear to curvilinear magnetic anomalies demarcating its southern boundary represented by the ~300 km-long Ketesso Shear Zone. The southern portion of the Sefwi Belt comprises the Sefwi-Wiawso Domain, which is characterised by NE- to ENE-striking high magnetic response from mafic to intermediate volcanic rocks, and low amplitude, low-frequency magnetic anomalies associated with multiple generations of pluton emplacement.

The broadest crustal architecture is defined by the contrasting geophysical signatures of the metasedimentary domains bounding the Sefwi Belt. The Sunyani-Comoé Domain is characterised by alternating high and low NE-striking magnetic domains (Fig. 2a, b). Smooth, low amplitude, long wavelength magnetic domains are associated with meta-sedimentary units bounded by highly magnetic linear anomalies interpreted as shear zones. Within the high magnetic domains, ENE-striking magnetic anomalies are coincident with metamorphosed volcano-sedimentary rocks, surrounding and along strike of elongate, elliptical magnetic lows associated with leucogranitic plutons. The Kumasi-Afema Domain, which has similar lithological associations to the Sunyani-Comoé Domain, is characterised by low- to moderate magnetic response with poorly developed NE-striking magnetic linear anomalies. All domains are cross-cut by Neoproterozoic NW-, NNW- and N-striking, dolerite dykes (Jessell, *et al.*, 2015, and references therein).

## 6. Tectono-metamorphic history

### 6.1 Deformation sequence

We distinguish five deformation events in the Sefwi Greenstone Belt and adjacent metasedimentary domains. The events are attributed to the Palaeoproterozoic Eburnean Orogeny. The framework for these five events is interpreted from field observations, kinematic analysis of aeromagnetic data and the macroscale geometries of discrete tectono-metamorphic domains.

#### 6.1.1 D<sub>1</sub>: NNW-SSE directed shortening

D<sub>1</sub> is defined by a ubiquitous, penetrative metamorphic foliation present in both high-grade rocks and low-grade rocks. Oblique to the regional architecture, the measured S<sub>1</sub> foliation within the Kukuom-Juaboso Domain is well imaged by highly magnetic E-W to ENE-WSW striking narrow anomalies. Where coincident with a sharp change in metamorphic grade and lithology, these anomalies are interpreted as D<sub>1</sub> shear zones, or thrust faults where kinematic indicators are observed. S<sub>1</sub> is defined by a shallowly- to steeply-dipping, schistose to gneissic foliation (Fig. 3), parallel to bedding (S<sub>0</sub>), forming the axial surface of poorly-preserved isoclinal, centimetric F<sub>1</sub> folds. Locally migmatitic intermediate orthogneisses display metamorphic banding dipping moderately (<60°) towards N330 to N350, with a down-dip hornblende stretching lineation and sheared leucosomes showing reverse top-to-the-SSE movement (Fig. 3a, b). Amphibolite facies packages of the Sefwi Belt and greenschist facies metasedimentary rocks of the Sunyani-Comoé Domain are separated by the Kenyase-Yamfo Shear Zone, however, D<sub>1</sub> kinematic indicators along the shear zone are largely obscured by later deformation and poor exposure.

In the Chiraa Domain, gneissic  $S_1$  trajectories follow an arcuate geometry, elongate toward  $\sim N250$ , constrained predominantly by field observations due to their corresponding weak magnetic response.  $S_1$  is defined by a biotite-rich foliation parallel to bedding in migmatitic garnet-bearing paragneiss (Fig. 3c), also observed in subordinate granitic orthogneiss. The shallow-dipping  $S_1$  is strongly overprinted by subsequent deformation transposing the foliation to moderately-dipping or subvertical with highly variable orientations (Fig. 3d).

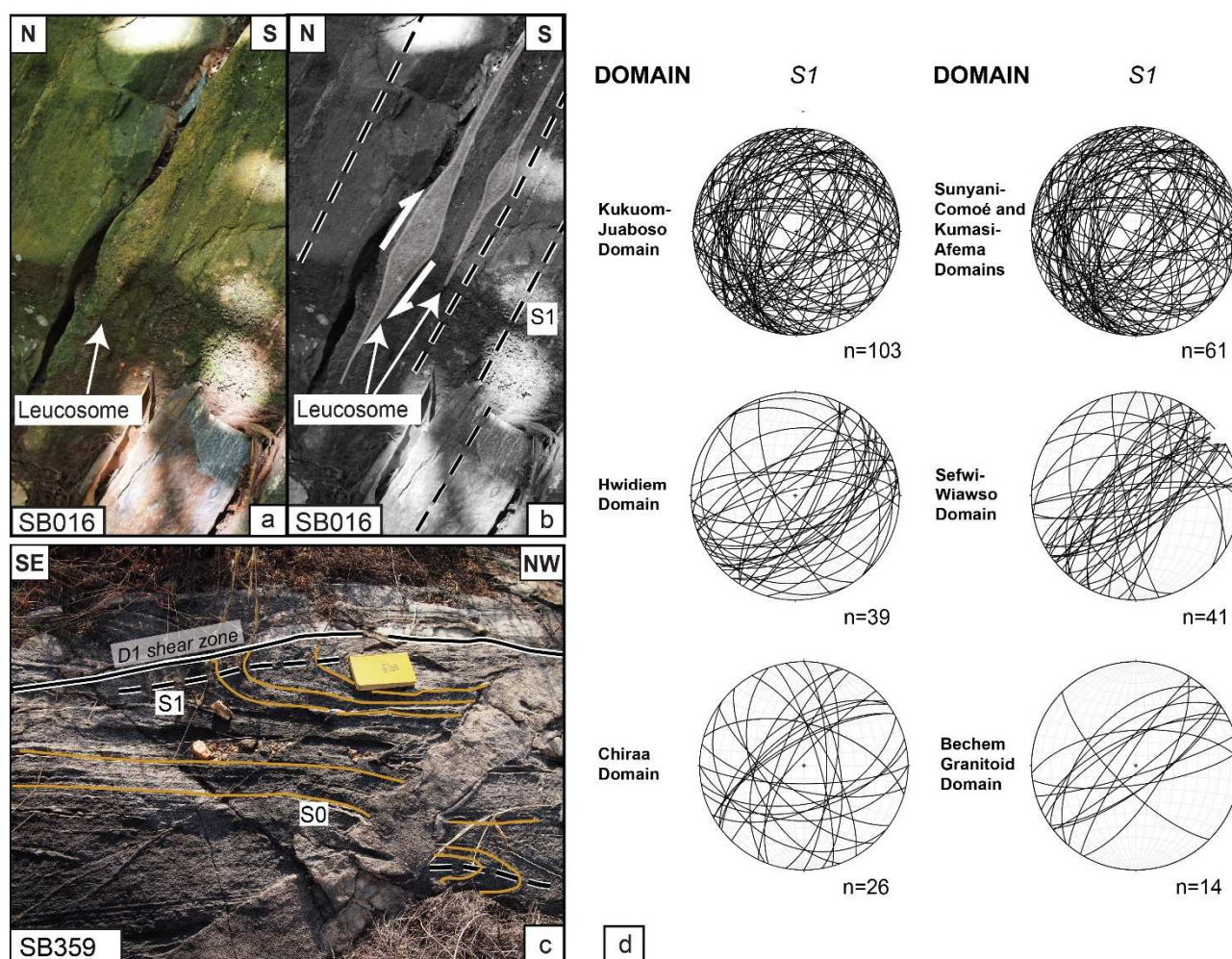


Fig. 3: Representative  $D_1$  structures in the study area showing key geometries and overprinting relationships (see Fig. 7 for outcrop locations). a) NNW-dipping gneissosity ( $S_1$ ) in a meta-andesite (SB016) in the Kukuom-Juaboso Domain with foliation-parallel, coarsely crystalline, late- $D_1$  leucosomes; b) Illustration highlights asymmetry of  $S_1$ -parallel leucosomes with steeply down-dip  $L_1$  amphibole stretching lineations (not shown) indicating reverse top-to-the-SSE kinematics; c) Bedding-parallel biotite foliation, axial planar to isoclinal  $F_1$  folds in a paragneiss unit (SB359) in the Chiraa Domain, showing low angle relationships with a  $D_1$  shear zone; d) Summary diagram of all  $S_1$  measurements from each domain plotted as a rose diagram to highlight structural trends.

similar to S<sub>1</sub>-parallel melt observed in the Kukuom-Juaboso Domain, suggesting partial melting occurred in both domains during or in the latter stages of D<sub>1</sub>.

In contrast, S<sub>1</sub> foliation trajectories in the low-grade metasedimentary domains, derived from field observations and parallel magnetic anomalies in the aeromagnetic surveys, define the axial surface of kilometre-scale NE-SW striking isoclinal folds of thick stratigraphic units, parallel to the crustal-scale shear zones that dominate the architecture. In the Sunyani-Comoé and Kumasi-Afema Domains, S<sub>1</sub> is characterised by a pervasive bedding parallel chlorite-white mica foliation in metasedimentary and volcano-sedimentary rocks, consistent with the bedding-parallel shear related fabric described by Allibone, *et al.* (2002a) in the Kumasi Group, in the southern Kumasi-Afema Domain. In mafic and intermediate meta-volcanic rocks of the Sefwi-Wiawso Domain, S<sub>1</sub> is characterised by a steeply dipping E-W to NE-SW, chlorite-actinolite-white mica schistosity in volcanic and volcanoclastite units or by mineral alignment in biotite- and hornblende-bearing granitoids, however, due to poor outcrop, no F<sub>1</sub> folds are identified.

Field evidence indicates D<sub>1</sub> deformation resulted in isoclinal folding, thrusting, high-grade metamorphism, and late-stage partial melting, consistent with lateral contractional deformation and crustal thickening during NNW-SSE directed shortening.

#### 6.1.2 D<sub>2</sub>: ENE-WSW directed transtension

D<sub>2</sub> deformation has a varied expression, depending on both the orientation of pre-existing structures and proximity to major D<sub>1</sub> shear zones. In the paragneisses of the Chiraa Domain, S<sub>2</sub> is axial planar to tight, gently-inclined to upright F<sub>2</sub> folds and is defined by a spaced biotite schistosity (Fig. 4a). F<sub>2</sub> fold axes are sub-parallel to L<sub>2</sub> mineral stretching lineations that are defined by elongate kyanite or biotite. The orientation of S<sub>2</sub> progressively rotates anticlockwise from ~N040 to N270, parallel to the arcuate geometries of the S<sub>1</sub> trajectories, steeply dipping in the northwest of the domain, and shallower to the south (60 - 80°S) (Fig. 5). In the far north of the domain, L<sub>2</sub> and F<sub>2</sub> plunging moderately (18–40°) towards the ~N230, rotating with the metamorphic fabric to an E-W orientation along the southern





Fig. 4. Representative  $D_2$  structures. a) Tight, SW plunging  $F_2$  folds in a garnet-biotite paragneiss in the Chiraa domain (SB440), refolding pelitic and psammitic layers ( $S_0$ ) and a bedding-parallel biotite foliation ( $S_1$ ); b) Migmatitic orthopyroxene-free garnet-clinopyroxene meta-basalt (SB177) on the southern margin of the Chiraa Domain, displaying subparallel relationship between  $S_2$  and transposed, refolded  $S_1$  foliation and plagioclase-rich leucosomes; c) Elongate, megacrystic garnet and

*clinopyroxene porphyroblasts and plagioclase-rich leucosomes (SB177); d) Open, constrictional F<sub>2</sub> fold refolding S<sub>1</sub> gneissosity in a migmatitic meta-basalt (SB089) in the Hwidiem Shear Zone, displaying a prominent L<sub>2</sub> stretching lineation parallel to the F<sub>2</sub> fold axis; e) L>>S tectonite in the Ketesso Shear Zone displaying pervasive mineral elongation in a quartz dioritic garnet amphibolite; f) Southeast dipping S-C<sub>2</sub> fabrics in the footwall of the Kenyase-Yamfo Shear Zone, associated with steeply east plunging L<sub>2</sub> stretching lineations, indicating normal, left-lateral movement; g) Prominent, NE-striking sub-vertical S<sub>2</sub> foliation in a pyritic, greenschist facies volcano-sedimentary rocks (SB103) in the Sunyani-Comoé Domain. S<sub>1</sub> and S<sub>2</sub> are orthogonally overprinted by a sub-vertical, N-striking dissolution cleavage (S<sub>3</sub>). Inset: h) Sub-vertical NE-striking S<sub>2</sub> crenulation cleavage overprinting a millimetric, flat-lying chlorite-white mica S<sub>1</sub> foliation.*

margin of the domain, plunging shallowly to moderately (~7–44°) towards both the east and west due to subsequent deformation. In the south of the domain, F<sub>2</sub> folds occur as centimetre-scale, rootless folds in migmatitic mafic orthogneisses (SB177) (Fig. 4b) displaying refolded leucosomes and elongation of clinopyroxene and garnet porphyroblasts (Fig. 4c). The southern and western extent of the Chiraa Domain are defined by the deflection and truncation of S<sub>1</sub>-parallel magnetic lineaments of the volcano-sedimentary schists of the Sunyani-Comoé Domain, characterised by NE-striking, alternating short wavelength, high amplitude and smooth, low amplitude magnetic signals. The interpreted boundary coincides with a significant change in metamorphic grade from migmatitic para- and orthogneisses to chlorite-white mica schists, each observed <1 km from the interpreted domain boundary, thus representing a sharp lateral metamorphic break. Both high- and low-grade rocks display moderately to steeply west-dipping S<sub>2</sub> foliations with shallow W- to SW-pitching L<sub>2</sub> stretching lineations. This contact is interpreted as a normal, oblique detachment fault, juxtaposing domains of contrasting metamorphic grade.

Within the Kukuom-Juaboso and Hwidiem domains, S<sub>1</sub> trajectories, corresponding D<sub>1</sub> magnetic fabrics and D<sub>1</sub> shear zones are refolded around tight F<sub>2</sub> folds elongate towards N230–N270. S<sub>2</sub> is a moderate- to steeply- (40–82°) NNW to SSE-dipping foliation defined by discontinuous biotite and/or amphibole (Fig. 5). F<sub>2</sub> fold hinges plunge 17–30° → ~N080, whilst L<sub>2</sub> amphibole stretching lineations plunge 9–36° between N065° and N109°. L<sub>2</sub> mineral stretching lineations in the centre of the Kukuom-Juaboso Domain plunge shallowly (7–34°) to the west, with more varied orientation proximal to domain boundaries due to later transposition. F<sub>2</sub> folds within the Hwidiem Shear Zone are open and upright, displaying prominent elongation and mineral stretching parallel to F<sub>2</sub> fold axes (Fig. 4d). This geometry indicates greater hinge parallel elongation relative to hinge-perpendicular shortening, which is characteristic of constrictional deformation (Dewey, *et al.*, 1998). L>>S tectonites in garnet-

amphibole-bearing dioritic amphibolites ( $L_2$ :  $4-11^\circ \rightarrow N230$ ) occur in the Ketesso high strain zone (Fig. 4e). Along strike, metre-scale boudin flow structures are observed in a strongly sheared, highly altered granite ( $L_2$ :  $11^\circ \rightarrow N225$ ). According to Sullivan (2013, and references therein),  $L \gg S$  and  $L$ -tectonites are indicative of transtension and ductile deformation in the mid- to lower crust. The observed coaxial relationship between ENE-WSW plunging  $L_2$  and  $F_2$ , their oblique orientation relative to the major NE-striking shear zones (Fossen, *et al.*, 2013; Sullivan, 2013) and the documentation of  $L \gg S$  tectonites are all consistent with constrictional deformation during ENE-WSW transtension.

High-amplitude  $D_1$  magnetic anomalies within the Kukuom-Juaboso Domain and the Hwidiem Shear Zone are deflected along, or occasionally truncated by, the >300km long, NE-striking magnetic lineament of the Kenyase-Yamfo Shear Zone.  $S_2$  foliations in the footwall metasediments of the Kenyase-Yamfo Shear Zone dip moderately to the south ( $\sim 48-64^\circ$ ) with an  $L_2$  mineral stretching lineation plunging  $\sim 52^\circ \rightarrow N092$ . Normal, left-slip kinematic indicators (Fig. 4f), which overprint the  $S_1$  foliation, suggest the shear zone was reactivated as a left-lateral normal fault during  $D_2$  ENE-WSW transtension.

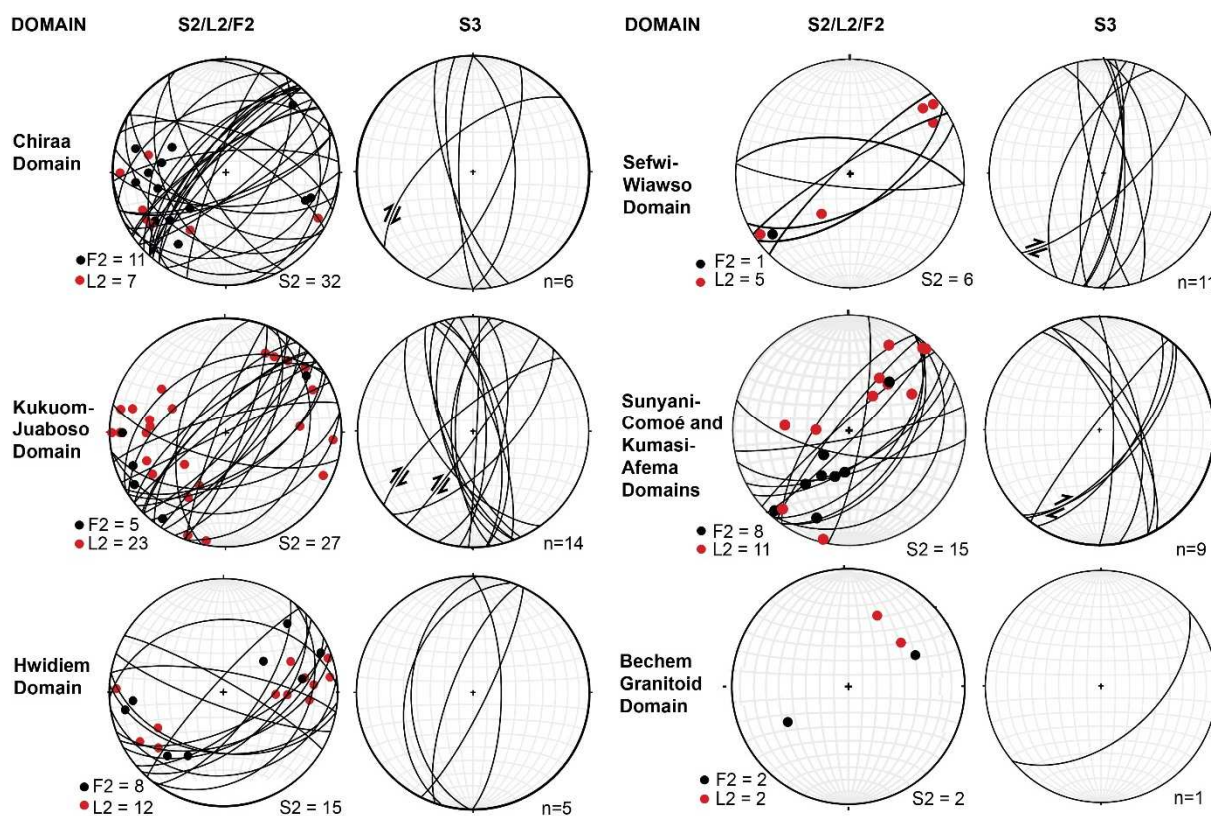


Fig. 5. Summary diagram of  $D_2$  and  $D_3$  structural data from domains within the study area. The first and third columns plot  $S_2$  planes and  $L_2$  and  $F_2$  poles to highlight the coaxial, shallow-plunging

*relationship of  $L_2$  and  $F_2$ . The second and fourth columns highlight the relatively consistent expression of  $D_3$  shortening throughout all domains.*

The metamorphic grade and  $F_2$  fold style associated with  $D_2$  deformation is variable between the Sefwi-Wiawso, Sunyani-Comoé and Kumasi-Afema domains. In the greenschist facies volcano-sedimentary rocks of the Sunyani-Comoé Domain,  $S_1$  is deformed by millimetre-scale, chevron style crenulations defining an upright axial planar  $S_2$  foliation (Fig. 4g, h), associated with metre-scale isoclinal folds.  $F_2$  fold hinges plunge shallowly to moderately (5 to  $\sim 40^\circ$ ) towards the southwest (Fig.5). Alternatively, the two earliest foliations locally form a sub-vertical NE-SW oriented, differential  $S_{1/2}$  cleavage parallel to the regional-scale shear zones. In the southern Sefwi-Wiawso Domain,  $F_2$  folds are rare, but are variably expressed as E-W to NE-SW striking axial traces, tight folds associated with spaced dissolution, crenulation cleavage or a weak chlorite schistosity. On the eastern margin of the domain, the NNE-striking brittle-ductile Bibiani Shear Zone separates folded meta-sedimentary rocks of the Kumasi-Afema domain in the footwall from polymictic conglomerates in the hanging wall and is interpreted as an extensional detachment. This is consistent with the truncation of  $D_1$  magnetic fabrics along the Bibiani Shear Zone during normal movement under  $D_2$  ENE-WSW transtension.

Despite the stress orientation undergoing little change between  $D_1$  and  $D_2$ , the deformation events are distinguished from one another on the basis of overprinting structural relationships, changes in metamorphic conditions and the exhumation of supracrustal rocks from depths of approximately 40km.  $D_1$  and  $D_2$ , therefore, represent a combination of multiphase deformation and progressive deformation (Fossen, *et al.*, 2018) and a shift from horizontal contractional deformation to horizontal constrictional deformation associated with sinistral transtension.

### *6.1.3 $D_3$ E-W directed shortening*

$D_3$  deformation is characterised by relatively homogeneous strain that transitions into focused simple shear-related deformation along narrow shear zones. In the Chiraa Domain,  $D_3$  deformation along the domain boundaries is associated with a localised greenschist facies metamorphic overprint of muscovite and chlorite after biotite and garnet, respectively. Internal to the domain,  $D_3$  is characterised by sub-vertical, N-S striking  $S_3$  crenulation cleavage (Fig. 5) with minor biotite recrystallization, axial planar to open, gently N-plunging  $F_3$  folds attributed to E-W shortening. The near orthogonal relationship between  $F_2$  and  $F_3$  fold axes has resulted in Type-3 fold interference patterns (Fig. 6a). Along the NE-striking western boundary of the Chiraa Domain, earlier fabrics are transposed to a sub-vertical orientation during localised dextral strike-slip movement (Fig. 6b). In the Kukuom-Juaboso

Domain, sinistral drag folds along metre-scale  $D_2$  faults are refolded by NNE-striking upright, gentle  $F_3$  folds (Fig. 6c).

In the low-grade metavolcanic and metasedimentary domains,  $D_3$  is characterised by a poorly developed N-S oriented dissolution cleavage distal to shear zones or a more pervasive NE-SW S-C fabric along NE-striking shear zones (Fig. 5). During  $D_3$ , pre-existing foliations ( $S_1$  and  $S_2$ ) become transposed proximal to domain boundaries and are rotated into sub-vertical orientations.

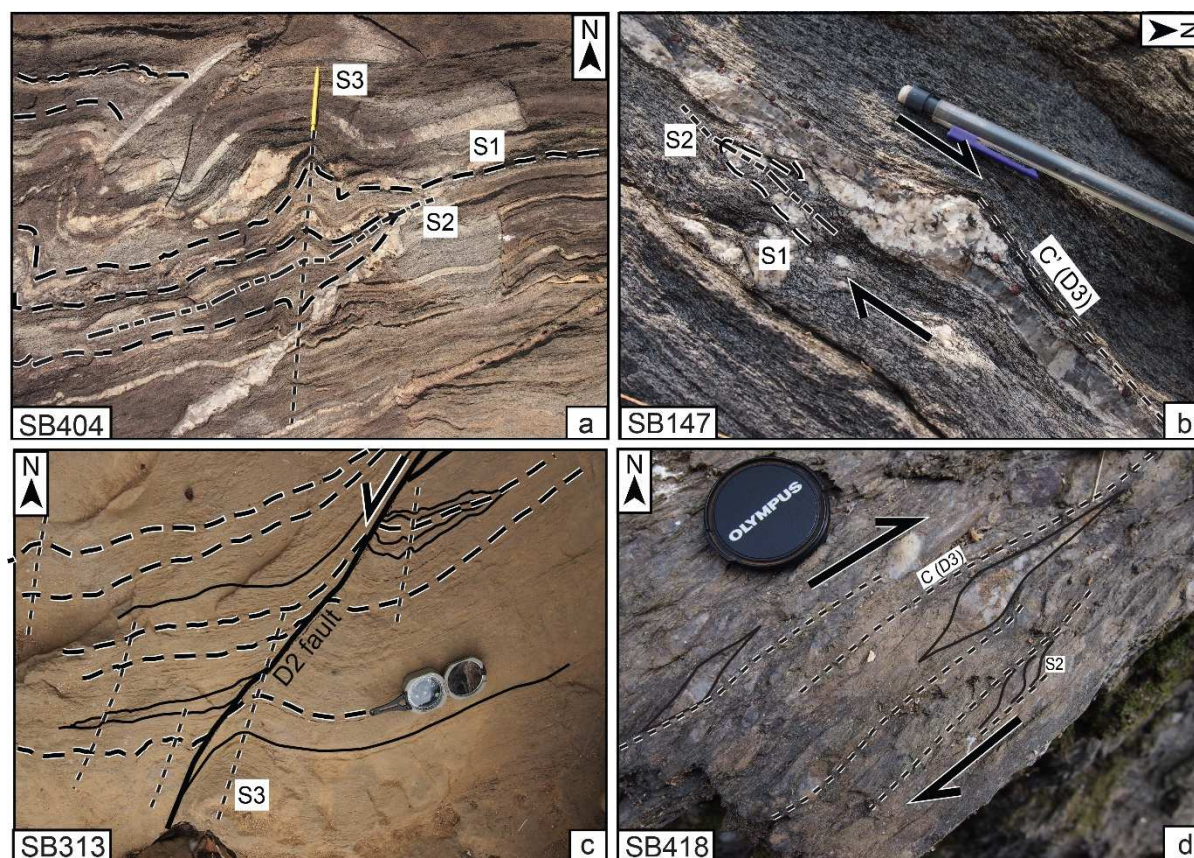


Fig. 6:  $D_3$  structures. a) Type-3 fold interference pattern in migmatitic paragneisses in the Chiraa Domain (SB404), illustrating the near orthogonal relationship of ENE-WSW oriented  $F_2$  folds and ~N-S striking  $S_3$  biotite foliations; b) Post-crystallisation dextral shearing of a garnet-bearing leucosome, sub-parallel to  $S_1$  and  $S_2$  foliations in a migmatitic paragneiss on the western margin of the Chiraa Domain (SB147); c) N- to NNE striking vertical  $S_3$  foliation overprinting drag folds generated during  $D_2$  sinistral strike-slip faulting in the southwestern regions of the Kukuom-Juaboso Domain (SB313); d) Prominently elongation of quartz clasts in Tarkwaian-type conglomerates and chlorite-white mica S-C<sub>3</sub> fabrics (SB418) indicating dextral shearing along the Ketesso Shear Zone.

In the high-strain Ketesso and Kenyase-Yamfo shear zones, chlorite-muscovite S-C<sub>3</sub> fabrics, sigmoidal asymmetries and sub-horizontal stretching lineations indicate dextral shearing under greenschist facies conditions. Sheared conglomerate clasts within the Ketesso Shear Zone indicate dextral movement

(Fig. 6d). Shear zones oriented at high angles to the principle E-W shortening field (e.g. NNE-striking Bibiani Shear Zone on the eastern boundary of the Sefwi Wiawso Domain) are not reactivated as strike-slip faults, and deformation is focused as W-over-E thrusting.

D<sub>3</sub> deformation in the airborne magnetic data sets is associated gentle N-S F<sub>3</sub> folds refolding early magnetic fabrics within the Kukuom-Juaboso, Hwidiem and Chiraa Domains, as well as the gentle refolding of the southern boundary of the Chiraa Domain. Within this dataset, the relative timing of dextral reactivation of major shear zones is interpreted from the truncations of anastomosing D<sub>2</sub> shear zones along more linear, high-amplitude, elongate NE-striking anomalies within the Ketesso, Kenyase-Yamfo and Afema shear zones. Overall we interpret D<sub>3</sub> to represent a progressive E-W directed shortening event in a strike-slip setting, indicating a tectonic switch after D<sub>2</sub> ENE-WSW transtension.

#### *6.1.4 D<sub>4</sub>: NW-SE shortening - Brittle ductile deformation and NNE-SSW sinistral shear zones*

D<sub>4</sub> is associated with NW-SE-directed shortening and brittle-ductile deformation. This deformation event did not significantly influence the macro-scale crustal architecture. D<sub>4</sub> generated sinistral oblique reactivation of the NNE-SSW Bibiani and Chirano shear zones, deflected existing fabric and faults in the Kumasi-Afema Domain. Pseudotachylites in the northern areas of the Bibiani Shear Zone crosscut an earlier east-west mineral foliation in a meta-dacite (SB051). Immediately west of the Chiraa Domain, NE-SW striking structures are truncated by a narrow NNE-SSW sinistral shear zone, with C<sub>4</sub>-S fabrics developed in a graphitic schist. In the aeromagnetic data, NNE-striking D<sub>4</sub> faults, including the reactivated Bibiani Shear Zone, truncate the Ketesso Shear Zone immediately to the north, whilst a smaller N-S shear zone west of Chiraa truncates reactivated D<sub>3</sub> shear zones in the Sunyani-Comoé Domain.

#### *6.1.5 D<sub>5</sub> WNW-ESE shortening; Reidel shear zones*

Late NW-SE, NE-SW and E-W oriented structures, which form conjugate fault sets developed during D<sub>5</sub> WNW-ESE shortening. Dextral displacement commonly observed along E-W striking shear zones and sinistral movement long NW-SE striking shear zones. Similar late-stage deformation was documented in neighbouring eastern Ivory Coast (e.g. Delor, *et al.*, 1992; Hirdes, *et al.*, 2007; Lüdtkke, *et al.*, 1999).

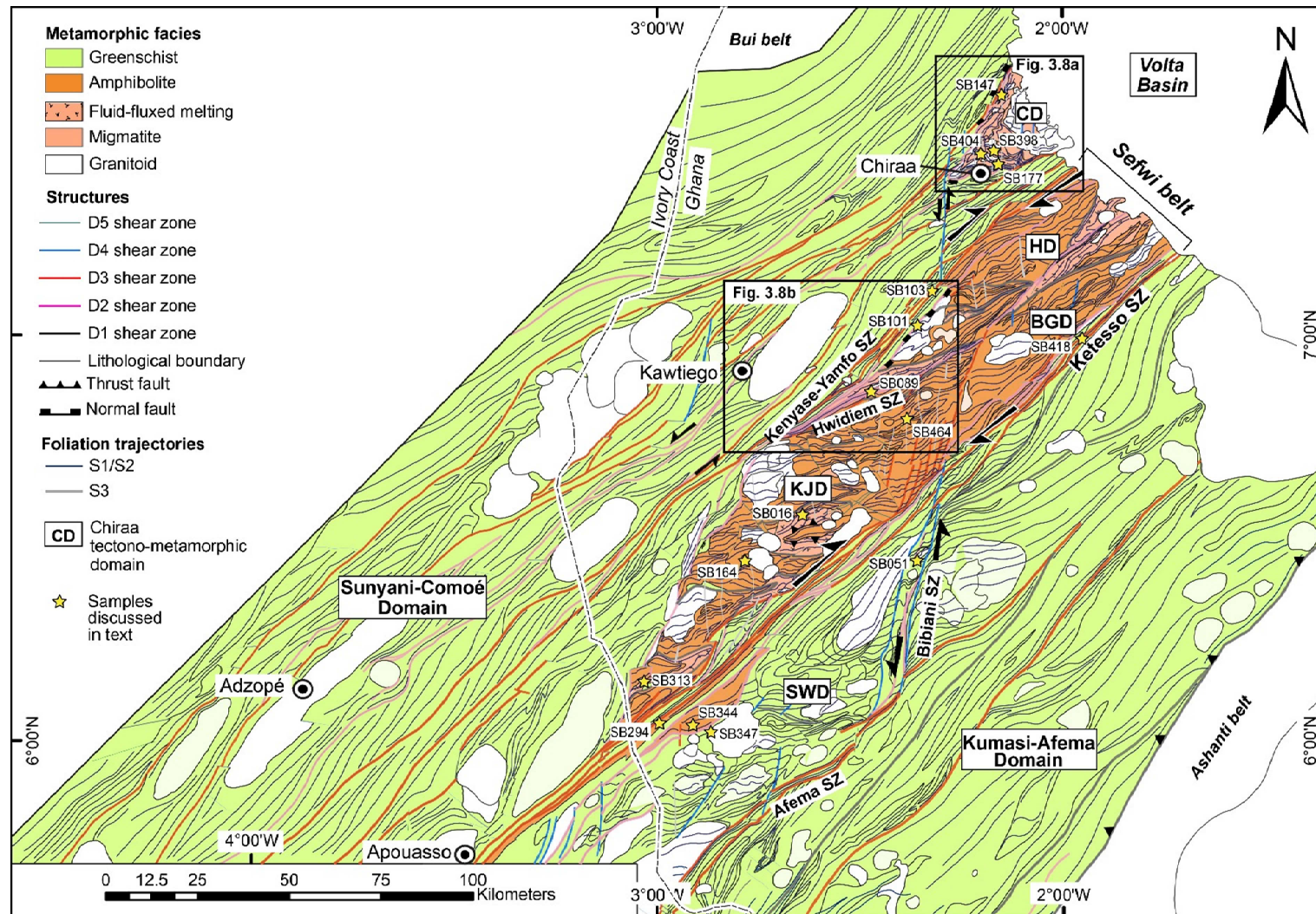


Fig. 7: Structural and metamorphic map of the study area displaying  $S_1$  foliation trajectories, major shear zones and the locations of samples mentioned in the text. Major shear zones display most recent fault movement, with the exception of the western boundary of the Chiraa Domain and the central segment of the Kenyase-Yamfo Shear Zone where normal movement and juxtaposition of domains of contrasting metamorphic grade during  $D_2$  are highlighted.  $S_3$  foliation trajectories are extrapolated from both field observations and interpretation of geophysical datasets.

The aeromagnetic expression of D<sub>5</sub> faults is interpreted from the truncation and lateral displacement of pre-existing linear magnetic anomalies. Faults are often localised, with a relatively short strike lengths less than 10 km.

## 6.2 Metamorphic history

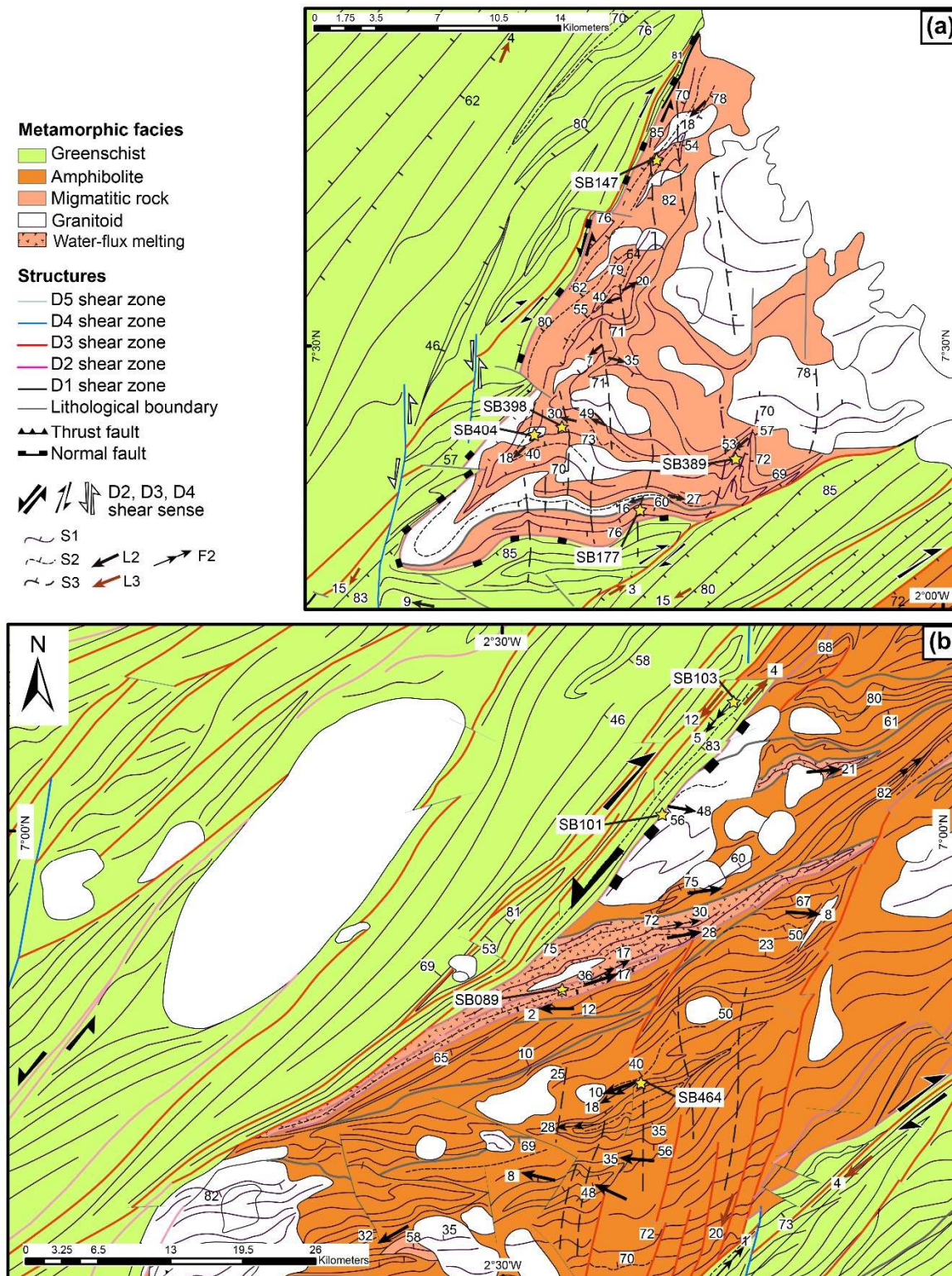
A new metamorphic map (Fig. 7) summarises the metamorphic grade of each domain based on field observations and petrographic analysis. A Grt-Ky-Bt paragneiss from the Chiraa Domain and a garnet amphibolite from the Kukuom-Juaboso Domain preserve prograde metamorphic conditions and peak pressure assemblages indicative of high-pressure amphibolite facies metamorphism (McFarlane, 2018). Prograde metamorphic conditions of 10.0–11.5 kbar, 580–650 °C (McFarlane, 2018), derived from pseudosections and garnet porphyroblast compositions, suggest cooler transient apparent geothermal gradients of 15–17 °C/km during the initial stages of orogenesis. Migmatitic paragneisses of the Chiraa Domain contain leucosomes parallel to the S<sub>1</sub> foliation that feed into cross cutting dilational leucocratic veins. Alternatively, a number of leucocratic dykes folded during D<sub>2</sub> preserve an axial planar S<sub>2</sub> foliation. This suggests that partial melting was late-D<sub>1</sub> to syn-D<sub>2</sub>. Suprasolidus assemblages and pseudosections indicate anatexis of rocks in the Chiraa Domain subsequent to crustal thickening is associated with increasing transient apparent geothermal gradients of 22–30 °C/km (McFarlane, 2018), reflecting thermal relaxation of the crust. . Congruent melting is not observed in the Kukuom-Juaboso Domain. Metamorphosed volcano-sedimentary rocks in the adjacent Sunyani-Comoé Domain preserve a peak greenschist facies assemblage of fine-grained chlorite-white mica ± actinolite. Retrograde clockwise P-T paths associated with a lower amphibolite facies metamorphic overprint in samples from the Chiraa and Kukuom-Juaboso domains indicate coeval decreases in pressure and temperature during exhumation (McFarlane, 2018). A pervasive, localised greenschist facies metamorphic overprint is observed along the boundaries of the high-grade domains and along major shear zones, subsequent to the exhumation and juxtaposition of domains of contrasting metamorphic grade.

The timing of the initiation of cooling and exhumation in the high-grade paragneisses (samples SB398 and SB389) is constrained by *in situ* monazite U-Pb SHRIMP ages of 2073 ± 2 Ma and 2074 ± 3 Ma (McFarlane, 2018). Monazite within the matrix are elongate parallel to S<sub>2</sub> or are parallel with the L<sub>2</sub> stretching lineation. The monazite age is interpreted as the timing of exhumation initiation, post-dating zircon U-Pb crystallisation ages of 2093 ± 2 Ma and 2092 ± 2 Ma from granites in the Chiraa Domain (Petersson, et al., 2016) and is consistent with many high-grade terranes where monazite populations are younger than zircon populations (Kelsey, *et al.*, 2008).



### 6.3 Structural-metamorphic map

The new tectono-metamorphic map illustrates the distribution of metamorphic facies with respect to the foliation trajectories (Fig. 7). It highlights the rhomboidal macro-geometries of the metamorphic domains within the study area. Migmatitic terranes preserving high-pressure mineral assemblages are interpreted as lower crustal segments.



*Fig. 8. (a) Detailed structural-metamorphic maps of the Chiraa Domain and (b) the intersection of the Hwidiem Shear Zone and the Kenyase Shear Zone (see Fig. 7 for locations). Juxtaposition of amphibolite facies and migmatitic rocks with greenschist facies volcano-sedimentary sequences occurs along normal oblique D2 faults, which are reactivated and transposed during D3 deformation.*

These are juxtaposed with amphibolite facies segments of the middle crust and greenschist facies metasedimentary domains, excluding the localised metamorphic overprint along shear zones, representing the upper crust. The map highlights the obliquity between the ENE-striking  $S_1$  foliation trajectories within the higher grade domains within the Chiraa Domain and the Sefwi Belt and the NE-striking trend of  $S_1$  trajectories in the adjacent low-grade domains. Overprinting relationships (Figs. 8a, b) demonstrate the low angle relationship between the strike of  $S_1$  and  $S_2$  and their concurrent rotation around the western and southern boundaries of the Chiraa Domain.

Figure 7 displays the less penetrative  $S_1$  foliation within granitoids within the Sefwi Belts as well as the deflection of foliation trajectories around leucogranites in the Sunyani-Comoé Domain. Sheared  $S_1$  foliation trajectories form regional scale S-C fabrics along strike of elongated leucogranitic plutons, which indicate sinistral movement along multiple  $D_2$  shear zones in the Sunyani-Comoé Domain. The NNE-to NE-striking western margins of the Chiraa and Kukuom-Juaboso domains coincide with the most significant lateral metamorphic breaks, which are attributed to extensional detachments developing under  $D_2$  ENE-WSW transtension. Based on the rhomboidal macrogeometries of the belt, field observations, structural measurements and the juxtaposition of domain of contrasting metamorphic grade, the present-day architecture is interpreted as the product of sinistral transtension. Interpretation of the Chiraa Domain as an extensional gneiss dome, according to the model of Rey, *et al.* (2017) does not sufficiently elucidate the significant lateral metamorphic breaks on the western and southern margins of the Chiraa and Kukuom-Juaboso domains, with the prevalence of transtensional folding and constrictional deformation between the Kenyase-Yamfo and Ketesso shear zones further contrasting the numerically modelled structures. The rotation of the  $S_1$  foliation in the Chiraa Domain and the normal oblique fault is instead interpreted as a regional-scale drag fold associated with left-lateral movement along the larger shear system (Figs. 8a).

$D_3$  E-W shortening is manifest in dextral shear-related geometries of magnetic anomalies along the northeast extent of the Kenyase-Yamfo Shear Zone, southeast of Chiraa, as well as the dextral rotation of a granitoid body north of Apouasso. Alternatively, N-S striking  $S_3$  foliation trajectories in the cores of the Kukuom-Juaboso and Chiraa domains are attributed to simple shear during  $D_3$ , distal to shear zones (Fig. 8b). Rocks of the Kukuom-Juaboso Domain are transected by and entrained in the  $D_3$  Ketesso high-strain zone, associated with a localised greenschist facies metamorphic overprint.

Foliation trajectories and major D<sub>3</sub> shear zones are truncated along NNE-striking D<sub>4</sub> shear zones, demonstrated by the truncation of the dextral Afema Shear Zone along the reactivated Bibiani Shear Zone and the sinistral displacement along an unnamed fault west of Chiraa which cross-cuts the Kenyase-Yamfo Fault. Similar truncations are observed along smaller faults within the Sunyani-Comoé Domain and in the southwestern extent of the Sefwi-Wiawso Domain.

The youngest structures attributed to D<sub>5</sub> WNW-ENE shortening are evident in the deflection of pre-existing foliation trajectories and shear zones along E-W striking dextral faults, less than 15 km in length, or, alternatively, as < 5 km NE-SW and NW-SE striking sinistral faults responsible for minor displacements.

## 7. Discussion

### 7.1 Timing of Eburnean deformation in SW Ghana

Many authors attribute tholeiitic and calc-alkaline volcanic, sodic plutonism and juvenile crust production to subduction and volcanic accretion during the Eburnean Orogeny or Eburnean I (2187-2158 Ma: Allibone, et al., 2002a; Feybesse, et al., 2006). Extensive reworking of the boundaries between the Sefwi Belt and the adjacent meta-sedimentary domains has hindered determination of the initial crustal architecture. Based on existing geochronological data, sedimentation in the Sunyani-Comoé and Kumasi-Afema Domains both yield an upper age limit of ca. 2159 Ma, which is derived from the youngest detrital zircon U-Pb age and syn-depositional volcanoclastite layers (Feybesse, et al., 2006; Oberthür, et al., 1998). Unlike the Sunyani-Comoé Domain, however, both the Sefwi Belt and the Kumasi-Afema Domain were intruded by alkali granites between ca. 2136 and 2130 Ma (Adadey, et al., 2009; Hirdes, et al., 2007), interpreted by some authors as evidence of an episode of lithospheric extension (Hirdes, et al., 2007), pre-dating our earliest deformation event. Despite a temporal overlap in the timing of sedimentation initiation, we suggest that the domains are not necessarily lateral equivalents and their initial relative spatial relationship is unknown (Fig. 9a).

Deformation and metamorphism in SW Ghana are attributed to the Eburnean Orogeny *sensu stricto* (Feybesse, et al., 2006). The timing of D<sub>1</sub> deformation and high-grade metamorphism documented in this study is not directly constrained, however, we propose that granite and leucogranite plutons emplaced between ca. 2093 and 2081 Ma along the northwest margin of the Sefwi Belt and in the Chiraa Domain (Hirdes, et al., 1992; Hirdes, et al., 2007; Petersson, et al., 2016) were produced during D<sub>1</sub> crustal thickening, thus providing a minimum age for D<sub>1</sub> (Fig. 9b). This is consistent with crustal thickening proposed by Feybesse, et al. (2006) for southern Ghana, which has been constrained

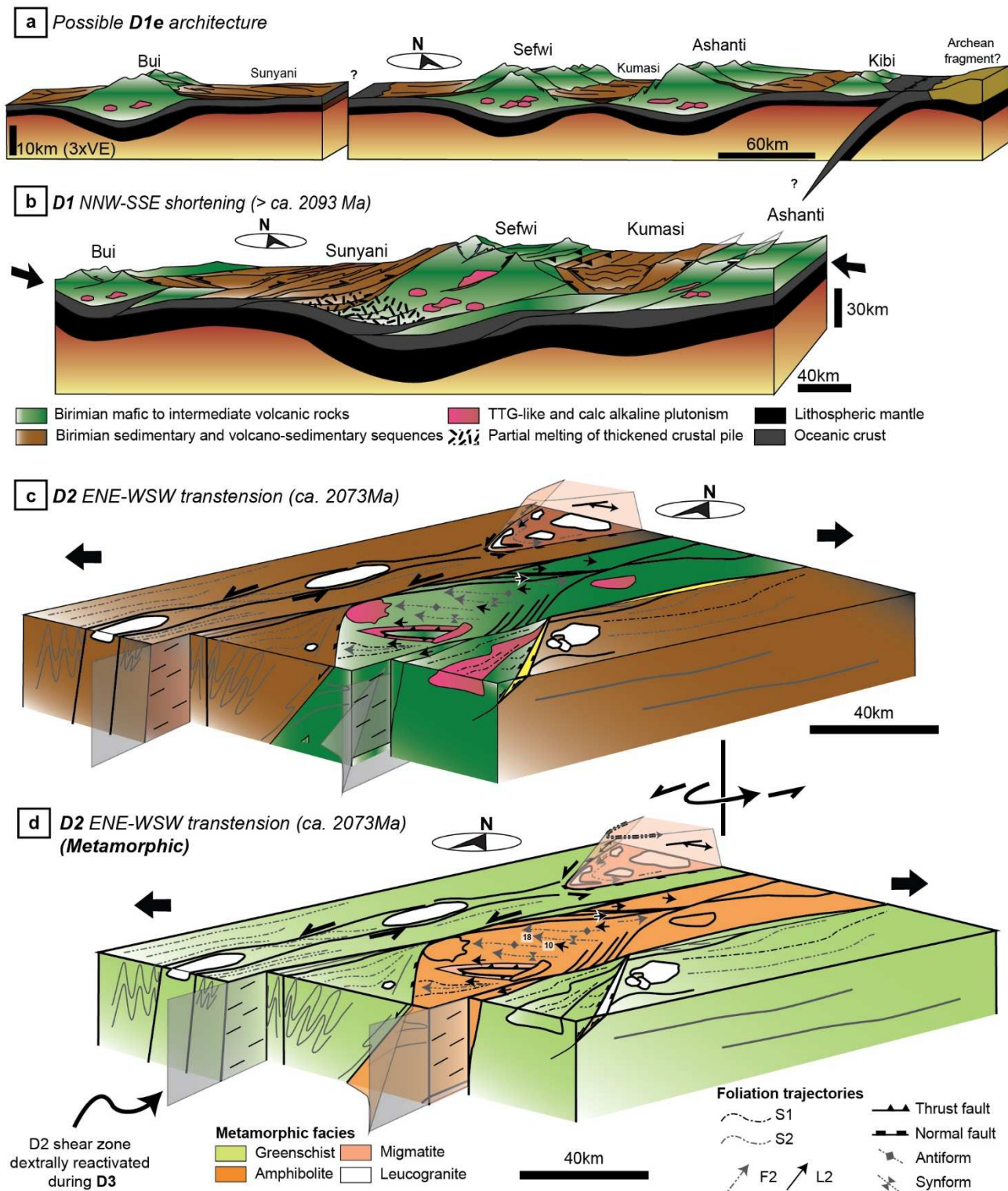


Fig. 9. a) Block diagram looking NNE illustrating the interpreted tectonic setting of greenstone belts prior to *D1*, highlighting the close spatial relationship between the Sefwi and Ashanti belts and an unknown distance between the Sunyani-Comoé Domain and the Sefwi Belt prior to *D1* collision; b) *D1* NNW-SSE shortening resulting in collision along the NW margin of the Sefwi belt, associated with folding and low angle thrust faults, crustal thickening and subsequent lower crustal anatexis. NB: change of scale and perspective for c & d; c) Block diagram of the initiation of *D2* ENE-WSW sinistral transtension (looking towards NNW). Figure displays the distribution of major lithological packages

*following the emplacement of leucogranites (ca. 2902 - 2081Ma) parallel to the NW margin of the Sefwi Belt within the Chiraa and the Sunyani-Comoé Domains, generated during D<sub>1</sub> anatexis. D<sub>2</sub> transtension results in the formation of grabens at high angles to major shear zones, or as narrow dilational jogs within shear zones, hosting conglomeratic Tarkwa-like units (yellow unit). Constrictional F<sub>2</sub> fold axis (grey trajectories) and L<sub>2</sub> stretching lineations (black arrows) within the Kukuom-Juaboso Domain display a coaxial relationship pitching shallowly to the WSW or to the ENE in the Hwidiem Shear Zone and Hwidiem Domain; d) Metamorphic block diagram highlighting the differential exhumation of high-grade rocks of the Chiraa and Kukuom-Juaboso domains relative to greenschist facies rocks of the Sunyani-Comoé Domain along west dipping detachments and NE-striking sinistral oblique shear zones. Schematic shows vorticity of drag fold of the western Chiraa Domain boundary under continued sinistral shear. Projected grey shear zones represent NE-SW striking structures transposed or reactivated during subsequent D<sub>3</sub> E-W shortening. D<sub>3</sub> deformation was progressively localised into these shear zones and was associated with a greenschist facies retrograde metamorphic overprint.*

by metamorphic monazite and vein-hosted zircon growth at  $2102 \pm 1$  Ma and  $2104 \pm 3$  Ma in the southern Ashanti Belt (Loh, et al., 1999).

The transition to D<sub>2</sub> transtension and associated lower crustal exhumation is constrained by monazite crystallisation ages at ca. 2073 Ma (McFarlane, 2018). The proposed timing of D<sub>2</sub> is consistent with the solid-state deformation and elongation (Jessell, et al., 2012) of ca. 2088 to 2081 Ma leucogranites (Hirdes, et al., 1992; Hirdes, et al., 2007) in the Sunyani-Comoé Domain. The close temporal spacing of these deformation events is consistent with the interpretation of D<sub>1</sub> and D<sub>2</sub> representing a combination of discrete deformations events and progressive deformation. Younger D<sub>3</sub> deformation was associated with greenschist facies metamorphism and dextral reactivation of the Sefwi shear system during E-W shortening. The timing of D<sub>3</sub> remains unconstrained. However, it is potentially correlated with retrograde greenschist facies metamorphism and hydrothermal xenotime crystallisation at  $2063 \pm 9$  Ma, which appears to post-date sinistral shearing in the Ashanti Belt (Pigois, et al., 2003). Previously described overprinting relationships and limited deformation expression form the basis for the relative timing of the youngest deformation events, D<sub>4</sub> and D<sub>5</sub>.

## *7.2 Rheology, tectonic style and exhumation*

The structural and metamorphic evolution of SW Ghana reflect a predominantly horizontal tectonic regime responsible for the formation and juxtaposition of tectono-metamorphic domains with contrasting metamorphic grade and deformation style. Heterogeneous crustal thickening and burial of supracrustal rocks during D<sub>1</sub> was accommodated by folding and low-angle thrust faults, associated with cooler apparent geothermal gradients, analogous to the early stages of modern collisional orogens (England & Thompson, 1984). We note, however, that whilst a number of authors propose crustal

thickening by nappe stacking along thrust faults (e.g. Allibone, *et al.*, 2002b; Feybesse, *et al.*, 2006; Milési, *et al.*, 1992), direct field evidence, such as inverted metamorphic gradients, is limited or often ambiguous.

Sporadic preservation of prograde HP-LT and HP-MT metamorphism associated with cooler apparent geothermal gradients (<15 °C/km) in both SW Ghana and NW Ghana (Block, *et al.*, 2015) indicates that localised areas of the West African Craton lithosphere were cool and strong enough to support moderate amounts of crustal thickening. This suggests development of thermo-mechanical properties similar to that of the Phanerozoic lithosphere (Rey & Houseman, 2006). Similar low apparent geothermal gradients and lateral deformation are documented in Archean greenstone belts of the East Pilbara Craton, which authors attribute to the downward advection, or *sagduction*, of cold, dense greenstone belts relative to upwelling, warm granitic domes (François, *et al.*, 2014; Thébaud & Rey, 2013). One of the primary arguments against the sagduction model for SW Ghana is the absence of voluminous granitoid intrusions adjacent to the high-pressure rocks, limiting density and viscosity contrasts in the lithospheric profile, therefore precluding initiation of sagduction. Similarly, a *hot-orogen* model does not sufficiently explain the strain patterns and metamorphism documented in southwest Ghana, which contrast the homogeneous lithospheric deformation, monotonous metamorphism and limited exhumation capacity of hot orogens proposed for Neoproterozoic and Palaeoproterozoic orogens (Cagnard, *et al.*, 2011; Cagnard, *et al.*, 2007; Chardon, *et al.*, 2009; Rey & Houseman, 2006), proposed also for areas of the West African Craton (e.g. Lompo, 2010; Vidal, *et al.*, 2009). Furthermore, geochronological data from SW Ghana indicates that D<sub>1</sub> and D<sub>2</sub> occurred within approximately 20 million years, suggesting the crust was not subjected to, or alternatively was unable to sustain, elevated geothermal gradients for prolonged periods of time.

Partial melting and increasing transient apparent geothermal gradients coincide with the end of D<sub>1</sub> crustal thickening, thermal relaxation of the crust and the transition from contractional to constrictional deformation during D<sub>2</sub>. D<sub>2</sub> deformation is characterised by shallow-pitching, WSW-oriented F<sub>2</sub> folds and coaxial, L<sub>2</sub> stretching lineations overprinting pre-existing low-angle D<sub>1</sub> structures. The obliquity between the regional NE-striking shear zones and coaxial L<sub>2</sub> lineations and F<sub>2</sub> fold axes is indicative of constrictional strain under a ENE-WSW transtensional regime (Dewey, *et al.*, 1998; Fossen, *et al.*, 2013). D<sub>2</sub> transtension resulted in the differential exhumation of high-grade tectono-metamorphic domains and their juxtaposition with low-grade domains occurred along NNE-striking normal detachments faults in association with normal sinistral reactivation of major NE-striking shear zones. Furthermore, we propose that the conglomerate and sandstone sequences west of the Bibiani

Shear Zone were deposited in NNE-striking half-graben structures that developed during D<sub>2</sub> transtension.

There are three possible interpretations of the driving force of constrictional strain, reflecting either a change in boundary conditions, waning convergent forces or the influence of gravitational forces (e.g. Chardon, et al., 2009; Duclaux, *et al.*, 2007). Within the *hot orogen* model, lateral constrictional flow develops during orogen-normal shortening in response to gravitational forces acting on thickened, hot lithosphere (Chardon, et al., 2009; Chardon, *et al.*, 2011; Cruden, *et al.*, 2006), similar to gravitational collapse of modern, wide, hot orogens (e.g. Brown, 2010; Royden, *et al.*, 2008; Vanderhaeghe & Teyssier, 2001). It is likely that partial melting of middle and lower crustal rocks documented in the northeast contributed to the localised rheological weakening of the crust. However, the observed metamorphic textures and calculated metamorphic *P-T* paths indicate concurrent cooling and exhumation (McFarlane, 2018), rather than isothermal decompression characteristic of gravitational collapse (e.g. Duchene, *et al.*, 2006). The evolution of strain documented in the Sefwi area bears some similarities to the numerical experiments and Archean tectono-metamorphic studies of Duclaux, et al. (2007), who propose that lessening convergent forces facilitate the transition from plane strain to constrictional deformation to accommodate gravitational forces. We propose, however, that constrictional deformation and late-orogenic exhumation reflect a shift from dominantly horizontal shortening to horizontal extension resulting transtensional strain. This is interpreted as a change in boundary conditions to ~ENE-WSW divergence, with deformation localised along a narrow, thickened orogenic belt with a partially molten lower crust. This thermo-mechanical behaviour and exhumation mechanism is partly analogous to exhumed Devonian UHP rocks in the Western Gneiss Region (western Norway) driven by the sinistral oblique plate divergence of Laurentian and Baltic plates (Krabbendam & Dewey, 1998).

The transition to E-W shortening during D<sub>3</sub> requires a significant switch in boundary conditions, resulting in the steepening and transposition of NNE-striking structures to sub-vertical orientations and the gentle refolding of older fabrics and structures oriented parallel to the shortening direction by folds < 10 km in wavelength, including the southern boundary of the Chiraa Domain, along which migmatitic rocks and low-grade schists were juxtaposed during D<sub>2</sub>. Horizontal chlorite L<sub>3</sub> stretching lineations along the Ketesso and Kenyase-Yamfo shear zones indicate a transition to a purely transcurrent tectonic regime with minimal vertical displacement during D<sub>3</sub>.

### 7.3 Orogenic model and regional correlations

Some of the major complexities when considering an orogenic model for the West African Craton arise from the craton-wide correlation of high-grade domains, meta-sedimentary rocks (proxy for basin formation) and deformation events. D<sub>1</sub> deformation in both the Sefwi and Ashanti Belts is attributed to N-S to NNW-SSE shortening, however, there is poor correlation in the timing of D<sub>1</sub> deformation. Whilst neither study directly dates the ~N-S shortening event, the Eoeburnean D<sub>1</sub> event of Perrouty, et al. (2012) between 2187 and 2158 Ma coincides with extensive calc-alkaline and TTG-like magmatism in the Sefwi Belt (Agyei Duodu, et al., 2009; Hirdes & Davis, 1998; Hirdes, et al., 1992). Other authors, however, suggest that initial thrust-related tectonism and crustal thickening in southwest Ghana occurred significantly later between ca. 2130 and 2105 Ma (Eisenlohr & Hirdes, 1992; Feybesse, et al., 2006; Milési, et al., 1992; Tunks, *et al.*, 2004).

Alternatively, polycyclic orogenic models for the West African Craton are inferred from exposures of high-grade terranes, interpreted to represent Palaeoproterozoic (>2150 Ma) basement deformed and metamorphosed prior the emplacement of the Birimian Supergroup and the Eburnean Orogeny *sensu stricto* (e.g. de Kock, et al., 2012; Hein, 2010; Pouclet, et al., 1996). In this study, the migmatitic paragneiss units of the Chiraa Domain represent supracrustal sequences buried to lower crustal depths during D<sub>1</sub>, forming the source of both the granitic melts found within the domain and the adjacent leucogranite plutons hosted by the Sunyani-Comoé Domain. This indicates that high-grade rocks of the Chiraa Domain do not represent the basement, but, instead, were formed and exhumed during the Eburnean Orogeny. Based on evidence of crustal thickening, coupled with the spatially restricted emplacement of the granitic melts and the metamorphic asymmetry of the study area, which increases in grade from south to north (Fig. 7), we propose that high-grade rocks of the Chiraa Domain formed during the collision between independent crustal segments comprising modern-day southern and central Ghana, with the northwest margin of the Sefwi Belt representing a narrow collisional front.

This interpretation is supported by discrepancies in the deformation sequence and the timing of deformation events documented in NW Ghana (Block, et al., 2015; 2016; de Kock, et al., 2011; 2012). Granite-greenstone terranes exposed in NW Ghana display evidence of thrust-related crustal thickening, high-grade metamorphism and anatexis during N-S shortening between ca. 2137 and 2127 Ma (Block, et al., 2015; 2016). Exhumation of the lower crust is attributed to gravitational collapse and N-S extension, overprinted by contractional deformation and continued crustal anatexis under E-W shortening between ca. 2123 and 2104 Ma. The authors propose that E-W shortening was generated by the collision of independent crustal blocks comprising NW Ghana (D<sub>3</sub>; Block, et al., 2016) and SW



Burkina Faso (D1; Baratoux, et al., 2011). Anatexis and high-grade metamorphism in NW Ghana commence ~40 million years prior to the genesis of collision-related leucogranites along the NW margin of the Sefwi Belt, indicating a diachronous metamorphic history for the high-grade terranes exposed in Ghana. However, the post-2110 Ma sinistral shearing along the N-S striking Jirapa shear zone of NW Ghana (D4: Block, et al., 2016) may represent a distal attenuation of the proposed collisional D<sub>1</sub> NNW-SSE shortening in SW Ghana.

We highlight that there is no change in the orientation in the strain regime between our D<sub>1</sub> and D<sub>2</sub> events, with deformation instead reflecting a shift from contractional to constrictional deformation associated with simple shear. Few direct correlations can be made between exhumation during D<sub>2</sub> ENE-WSW sinistral transtension described in this study and deformation described in adjacent terranes. Transtension was invoked for the opening of the Haute-Comoé Basin in eastern Ivory Coast (Vidal & Alric, 1994), representing an extension of the Sunyani-Comoé Domain, however, we do not deem this to be the equivalent of our D<sub>2</sub> which exhumes lower crustal rocks relative to deformed and metamorphosed metasedimentary rocks of the Sunyani-Comoé Domain. Migmatitic paragneisses exposed on the eastern flank of the Ashanti Belt are interpreted as deeper crustal segments metamorphosed at ca. 2100 Ma (John, et al., 1999; Loh, et al., 1999), however, the structural and temporal context of the exhumation of the terrane is unknown. Our D<sub>2</sub> potentially correlates with the sinistral reactivation of the Ashanti fault during NNW-SSE shortening (D4: Perrouy, et al., 2012), however, this cannot be substantiated without further precise age dating of deformation in the Ashanti Belt. We emphasise that D<sub>2</sub> transtension and lower crust exhumation documented in this study is not equivocal to the D<sub>2</sub> extension event of Perrouy, et al. (2012), which is responsible for basin formation. Better correlation is found between deformation events D<sub>4</sub> and D<sub>5</sub> of NW Ghana occurring after ca. 2110 Ma (Block, et al., 2016), and the proposed collision of southern Ghana and northern Ghana (D<sub>1</sub>; this study). Both reveal sinistral shear zones overprinted by dextral NE-striking strike-slip shear zones during E-W shortening (D5; Block, et al., 2016). Such deformation may be the distal expression of the terminal collision of the Archaean Kénéma-Man Domain and the Baoulé-Mossi domain between 2050 and 2030 Ma (Kouamelan, *et al.*, 1997; Pitra, et al., 2010).

Paleogeographic and geochronological reconstructions have provided evidence that West Africa and the São Luís Craton were contiguous during the Palaeoproterozoic (e.g. Hurley, *et al.*, 1967; Klein & Moura, 2008, and references therein; Torquato & Cordani, 1981). Magmatism of the São Luís craton and the basement of the Gurupi belt is defined by three periods of magmatic activity ( $2240 \pm 5$  Ma;  $2160 \pm 10$  Ma;  $2080 \pm 20$  Ma), sharing lithological and structural characteristics with SW Ghana (Klein & Moura, 2008, and references therein), including peraluminous collision-type granitoids (2086

– 2090 Ma), produced by partial melting during collision (Klein, *et al.*, 2005; Klein & Moura, 2008). Similarly, the Ile de Cayenne Complex of French Guiana is characterised by early tholeiitic to calc-alkaline magmatism followed by emplacement of TTG magmas between ca. 2174 and 2144 Ma (Delor, *et al.*, 2003; Feybesse, *et al.*, 2006; Hirdes, *et al.*, 2007; Vanderhaeghe, *et al.*, 1998). Crustal thickening, anatexis and emplacement of ca. 2093 and 2083 Ma potassic granitoids and peraluminous leucogranites along major shear zones in French Guiana is attributed to oblique collision and late orogenic lateral extrusion (Kroonenberg, *et al.*, 2016; Vanderhaeghe, *et al.*, 1998), potentially representing the lateral equivalents of events recorded in southwest Ghana. The final correlation between the two terranes comes from the timing of crustal extension and formation of granulite facies metamorphism in the Guiana Shield between ca. 2070 to 2060 Ma (Delor, *et al.*, 2001), which we interpret to be a lateral continuation of the D<sub>2</sub> deformation and metamorphism recorded on the northwest margin of the Sefwi Belt. The sinistral movement of major shear zones places modern-day SW Ghana, adjacent to the São Luís Craton, in NE Brazil and French Guiana Shield in Nuna reconstructions.

In summary, structural and metamorphic evidence from SW Ghana indicate heterogeneous crustal thickening and clockwise *P-T-t* paths reminiscent of modern collisional orogens. Collisional orogenesis and the exhumation of middle and lower crust documented in both NW Ghana and SW Ghana occur more than 40 million years apart. Such large discrepancies in the timing of deformation and metamorphism are more consistent with episodic collisional orogenesis, supporting a growing body of research suggesting collision between discrete Palaeoproterozoic terranes in the West African Craton (Block, *et al.*, 2016; Parra-Avila, 2015; Parra-Avila, *et al.*, 2016). Furthermore, coeval granite-greenstone terranes of southern Ghana, the Sao Luis Craton and French Guiana demonstrate comparable magmatic and tectono-thermal evolutions during the formation and accretion of juvenile terranes, pointing towards a common, laterally contiguous tectonic setting.

#### *7.4 Implications for Palaeoproterozoic tectonics*

Palaeoproterozoic rocks of the West African Craton provide an opportunity to explore the evolution of orogenic processes in a terrane characterised by Archean-like granite-greenstone associations and craton-scale shear zones. The episodic collisional orogenic model proposed for the West African Craton requires the rapid formation and accretion of independent, juvenile Palaeoproterozoic terranes. Structural and metamorphic analysis of SW Ghana reveals characteristics akin to subduction-related accretion-collision processes that typify Phanerozoic orogens (e.g. van Staal, *et al.*, 2009; Windley, *et al.*, 2007). The diachronous timing of deformation and metamorphism,

discrepancies in deformation histories and the absence of lateral age gradients hints at the coeval operation of multiple, subduction zones. We emphasise, however, that an episodic collisional model does not require individual subduction zones for each greenstone belt. Some authors propose analogous tectonic models for Archean provinces including the Barberton terrain (Diener, *et al.*, 2013; Moyen, *et al.*, 2006) and the Abitibi Subprovince (Daigneault, *et al.*, 2002; Mueller, *et al.*, 1996), suggesting these processes have been active since the Archean.

The broader crustal architecture of southern Ghana, coupled with newly presented structural and metamorphic data, does not conform with the dome and keel geometries of Archean greenstone terranes (François, *et al.*, 2014; Van Kranendonk, *et al.*, 2007), nor support burial and exhumation by sagduction (François, *et al.*, 2014; Thébaud & Rey, 2013). In the West African Craton, sporadic preservation of peak metamorphic pressure of 10–14 kbar associated with cooler apparent geothermal gradients (Block, *et al.*, 2015; Ganne, *et al.*, 2012; Pitra, *et al.*, 2010) suggest that the lithosphere of sufficient rheological strength to support heterogeneous crustal thickening and burial of supracrustal sequences. Transtension-related exhumation of HP rocks in SW Ghana are comparable to the exhumed Devonian UHP rocks of the Scandinavian Caledonides (Krabbendam & Dewey, 1998). Homogeneous deformation and laterally monotonous metamorphism in the younger Southern Finnish Svecofennides is attributed to the *hot orogen* model (Cagnard, *et al.*, 2007; Väisänen & Hölttä, 1999), contrasting the proposed episodic collisional model for the WAC, suggesting non-uniformity in Palaeoproterozoic lithospheric thermo-mechanical properties and orogenic processes, therefore, illustrating the progressive, diachronous adoption of a modern, subduction-driven orogenesis.

## 8. Conclusions

A new interpretation of the litho-tectonic architecture, combined with the regional structural framework and complementary metamorphic data suggests that the domains within the Sefwi Belt record significant heterogeneous crustal thickening during NNW-SSE shortening. The tectonic contact between the Sefwi Belt and the Sunyani-Comoé Domain is interpreted as a narrow, collisional front, representing a suture zone between SW Ghana and central Ghana/Ivory Coast that formed during oblique convergence. The transition from D<sub>1</sub> to D<sub>2</sub> coincides with a shift from contractional to constrictional deformation and the development of a transcurrent tectonic regime. Based on previous studies of elongate granites coupled with macro-geometries of domains, we interpret major normal, left-lateral movement within the Sefwi shear system. Differential exhumation of high-grade domains occurred after thermal relaxation of the orogenic crust during D<sub>2</sub> ENE-WSW transtension, contrasting the surface geology predicted for Precambrian hot orogens. Structural and metamorphic evidence

indicate that transtension is the product of orogenic extension reflecting changes in boundary conditions and oblique plate divergence, with partial melting and localised rheological weakening of the lower crust representing a subordinate contributing factor. Dextral reactivation of NE-striking shear zones is attributed to the final major deformation event reflects a switch in far-field boundary conditions. We highlight the diachronous nature of high-grade metamorphism and discrepancies in deformation histories across the craton during the Eburnean Orogeny, which we interpret as the product of episodic collisional orogenesis between discrete juvenile terranes during the assembly and stabilisation of the West African Craton.

## 9. Acknowledgements

We wish to gratefully acknowledge AMIRA International and the industry sponsors, including AusAid and the ARC Linkage Project LP110100667, for their support of the WAXI project (P934A). Field expenses were funded by the School of Earth, Atmosphere and Environment, Monash Research Initiative Fund – Dr L. Ailleres. We acknowledge the facilities and technical staff at the Monash Centre for Electron Microscopy. Special thanks are extended to the Geological Survey Department of Ghana for logistical support in the field and additional data, including chauffeurs K. Duah. Datasets used included regional airborne magnetic and radiometric data covering SW Ghana were acquired by the Geological Survey Department of Ghana and GoldenStar Resources Pty Ltd.

## 10. References

- Abouchami, W., Boher, M., Michard, A. & Albarede, F., 1990. A major 2.1 Ga event of mafic magmatism in West Africa: an early stage of crustal accretion. *Journal of Geophysical Research*, **95**(B11), 17,605-17,629.
- Adadey, K., Clarke, B., Théveniaut, H., Urien, P., Delor, C., Roig, J. Y. & Feybesse, J. L., 2009. Geological Map Explanation - Map Sheet 0503B (1:100 000), CGS/BRGM/Geoman. Geological Survey Department of Ghana (GSD).
- Agyei Duodu, J., Loh, G. K., Boamah, K. O., Baba, M., Hirdes, W., Toloczyki, M. & Davis, D. W., 2009. Geological Map of Ghana 1:1 000 000, Geological Survey Department, Accra, Ghana.
- Aitken, A. R. A. & Betts, P. G., 2009. Multi-scale integrated structural and aeromagnetic analysis to guide tectonic models: An example from the eastern Musgrave Province, Central Australia. *Tectonophysics*, **476**(3–4), 418-435.
- Allibone, A., McCuaig, T., Harris, D., Etheridge, M., Munroe, S., Byrne, D., Amanor, J. & Gyapong, W., 2002a. Structural controls on gold mineralization at the Ashanti deposit, Obuasi, Ghana. *Special Publication - Society of Economic Geologists*, **9**, 65-94.
- Allibone, A., Teasdale, J., Cameron, G., Etheridge, M., Uttley, P., Soboh, A., Appiah-Kubi, J., Adanu, A., Arthur, R., Mamphey, J., Odoom, B., Zuta, J., Tsikata, A., Pataye, F., Famiyeh, S. & Lamb, E., 2002b. Timing and structural controls on gold mineralization at the Bogoso Gold Mine, Ghana, West Africa. *Economic Geology*, **97**(5), 949-969.
- Amponsah, P. O., 2012. *Multiscale structural analysis of the Sunyani basin, Ghana*. Unpub. MSc Thesis, Department of Earth Science, University of Ghana. pp. 107.

- Baratoux, L., Metelka, V., Naba, S., Jessell, M. W., Grégoire, M. & Ganne, J., 2011. Juvenile Paleoproterozoic crust evolution during the Eburnean orogeny (~2.2 - 2 Ga), western Burkina Faso. *Precambrian Research*, **191**(1–2), 18–45.
- Bessoles, B., 1977. Géologie de l’Afrique. Le craton Ouest-Africain, pp. 88, Mémoires BRGM, Paris.
- Betts, P., Williams, H., Stewart, J. & Aillères, L., 2007. Kinematic analysis of aeromagnetic data: Looking at geophysical data in a structural context. *Gondwana Research*, **11**(4), 582–583.
- Béziat, D., Bourges, F., Debat, P., Lompo, M., Martin, F. & Tollon, F., 2000. A Paleoproterozoic ultramafic-mafic assemblage and associated volcanic rocks of the Boromo greenstone belt: fractionates originating from island-arc volcanic activity in the West African craton. *Precambrian Research*, **101**(1), 25–47.
- Bhattacharya, S., 2004. High-temperature crustal scale shear zone at the western margin of the Eastern Ghats granulite belt, India: implications for rapid exhumation. *Journal of Asian Earth Sciences*, **24**(3), 281–290.
- Billa, M., Feybesse, J. L., Bronner, G., Lerouge, C., Milési, J. P., Traoré, S. & Diaby, S., 1999. Banded ferruginous quartzite formations of the Nimba and Simandou ranges: Tectonically stacked units on an Archean plutonic 'basement' (Kenema-Man craton), during the Eburnean orogeny. *Les formations a quartzites rubanes ferrugineux des Monts Nimba et du Simandou : Des unites empilees tectoniquement, sur un 'soubassement' plutonique Archeen (craton de Kenema-Man), lors de l'orogene Eburneen*, **329**(4), 287–294.
- Block, S., Ganne, J., Baratoux, L., Zeh, A., Parra - Avila, L. A., Jessell, M., Aillères, L. & Siebenaller, L., 2015. Petrological and geochronological constraints on lower crust exhumation during Paleoproterozoic (Eburnean) orogeny, NW Ghana, West African Craton. *Journal of Metamorphic Geology*, **33**(5), 463–494.
- Block, S., Jessell, M., Aillères, L., Baratoux, L., Bruguier, O., Zeh, A., Bosch, D., Caby, R. & Mensah, E., 2016. Lower crust exhumation during Paleoproterozoic (Eburnean) orogeny, NW Ghana, West African Craton: Interplay of coeval contractional deformation and extensional gravitational collapse. *Precambrian Research*, **274**, 82–109.
- Boher, M., Abouchami, W., Michard, A., Albarede, F. & Arndt, N. T., 1992. Crustal growth in West Africa at 2.1 Ga. *Journal of Geophysical Research: Solid Earth*, **97**(B1), 345–369.
- Bonhomme, M., 1962. Contribution à l'étude géochronologique de la plate-forme de l'Ouest Africain. *Annals de la Faculté des Sciences de Université de Clermont-Ferrand Géol. Minéral*, **5**, 62.
- Bouhallier, H., Chardon, D. & Choukroune, P., 1995. Strain patterns in Archean dome-and-basin structures: The Dharwar craton (Karnataka, South India). *Earth and Planetary Science Letters*, **135**(1), 57–75.
- Brown, M., 2006. Duality of thermal regimes is the distinctive characteristic of plate tectonics since the Neoproterozoic. *Geology*, **34**(11), 961–964.
- Brown, M., 2007. Metamorphic Conditions in Orogenic Belts: A Record of Secular Change. *International Geology Review*, **49**(3), 193–234.
- Brown, M., 2010. Melting of the continental crust during orogenesis: the thermal, rheological, and compositional consequences of melt transport from lower to upper continental crust. *Canadian Journal of Earth Sciences*, **47**(5), 655–694.
- Caby, R., Delor, C. & Agoh, O., 2000. Lithologie, structure et métamorphisme des formations birimiennes dans la région d'Odienné (Côte d'Ivoire): rôle majeur du diapirisme des plutons et des décrochements en bordure du craton de Man. *Journal of African Earth Sciences*, **30**(2), 351–374.
- Cagnard, F., Barbey, P. & Gapais, D., 2011. Transition between “Archean-type” and “modern-type” tectonics: Insights from the Finnish Lapland Granulite Belt. *Precambrian Research*, **187**(1), 127–142.
- Cagnard, F., Durrieu, N., Gapais, D., Brun, J.-P. & Ehlers, C., 2006. Crustal thickening and lateral flow during compression of hot lithospheres, with particular reference to Precambrian times. *Terra Nova*, **18**(1), 72–78.
- Cagnard, F., Gapais, D. & Barbey, P., 2007. Collision tectonics involving juvenile crust: The example of the southern Finnish Svecofennides. *Precambrian Research*, **154**(1–2), 125–141.
- Calvert, A., Sawyer, E., Davis, W. & Ludden, J., 1995. Archean subduction inferred from seismic images of a mantle suture in the Superior Province. *Nature*, **375**(6533), 670.
- Cawood, P. A., Kroner, A. & Pisarevsky, S., 2006. Precambrian plate tectonics: criteria and evidence. *GSA Today*, **16**(7), 4.

- Chardon, D., Gapais, D. & Cagnard, F., 2009. Flow of ultra-hot orogens: A view from the Precambrian, clues for the Phanerozoic. *Tectonophysics*, **477**(3–4), 105-118.
- Chardon, D., Jayananda, M. & Peucat, J. J., 2011. Lateral constrictional flow of hot orogenic crust: insights from the Neoproterozoic of south India, geological and geophysical implications for orogenic plateaux. *Geochemistry, Geophysics, Geosystems*, **12**(2).
- Chopin, C., 2003. Ultrahigh-pressure metamorphism: tracing continental crust into the mantle. *Earth and Planetary Science Letters*, **212**(1), 1-14.
- Choukroune, P., Bouhallier, H. & Arndt, N., 1995. Soft lithosphere during periods of Archaean crustal growth or crustal reworking. *Geological Society, London, Special Publications*, **95**(1), 67-86.
- Collins, A. S., Reddy, S. M., Buchan, C. & Mruma, A., 2004. Temporal constraints on Palaeoproterozoic eclogite formation and exhumation (Usagaran Orogen, Tanzania). *Earth and Planetary Science Letters*, **224**(1), 175-192.
- Condie, K. C., 1994. Greenstones through time. *Developments in Precambrian Geology*, **11**, 85-120.
- Condie, K. C. & Kröner, A., 2008. When did plate tectonics begin? Evidence from the geologic record. *Geological society of America special papers*, **440**, 281-294.
- Cruden, A. R., Nasserli, M. H. & Pysklywec, R., 2006. Surface topography and internal strain variation in wide hot orogens from three-dimensional analogue and two-dimensional numerical vice models. *Geological Society, London, Special Publications*, **253**(1), 79-104.
- Daigneault, R., Mueller, W. U. & Chown, E. H., 2002. Oblique Archean subduction: accretion and exhumation of an oceanic arc during dextral transpression, Southern Volcanic Zone, Abitibi Subprovince Canada. *Precambrian Research*, **115**(1–4), 261-290.
- Dampare, S. B., Shibata, T., Asiedu, D. K., Osa, S. & Banoeng-Yakubo, B., 2008. Geochemistry of Paleoproterozoic metavolcanic rocks from the southern Ashanti volcanic belt, Ghana: Petrogenetic and tectonic setting implications. *Precambrian Research*, **162**(3-4), 403-423.
- Davis, D. W., Hirdes, W., Schaltegger, U. & Nunoo, E. A., 1994. U-Pb age constraints on deposition and provenance of Birimian and gold-bearing Tarkwaian sediments in Ghana, West Africa. *Precambrian Research*, **67**(1-2), 89-107.
- de Kock, G. S., Armstrong, R. A., Siegfried, H. P. & Thomas, E., 2011. Geochronology of the Birim Supergroup of the West African craton in the Wa-Bolé region of west-central Ghana: Implications for the stratigraphic framework. *Journal of African Earth Sciences*, **59**(1), 1-40.
- de Kock, G. S., Théveniaut, H., Botha, P. M. W. & Gyapong, W., 2012. Timing the structural events in the Palaeoproterozoic Bolé–Nangodi belt terrane and adjacent Maluwe basin, West African craton, in central-west Ghana. *Journal of African Earth Sciences*, **65**(0), 1-24.
- de Wit, M. J., de Ronde, C. E. J., Tredoux, M., Roering, C., Hart, R. J., Armstrong, R. A., Green, R. W. E., Peberdy, E. & Hart, R. A., 1992. Formation of an Archaean continent. *Nature*, **357**(6379), 553-562.
- Debat, P., Nikiéma, S., Mercier, A., Lompo, M., Béziat, D., Bourges, F. B., Roddaz, M., Salvi, S., Tollon, F. & Wenmenga, U., 2003. A new metamorphic constraint for the Eburnean orogeny from Paleoproterozoic formations of the Man shield (Aribinda and Tampilga countries, Burkina Faso). *Precambrian Research*, **123**(1), 47-65.
- Delor, C., Diaby, I., Simeon, Y., Adou, M., Zamble, Z., Tastet, J.-P., Yao, B., Konan, G., Chiron, J.-C. & Dommanget, A., 1992. Carte Géologique de la Côte d'Ivoire à 1/200 000, Feuille Grand-Bassam, Direction de la Géologie, Abidjan, Côte d'Ivoire.
- Delor, C., Lafon, J.-M., Lahondere, D., de Roeber, E., Fraga, M. L., Rossi, P. & Potrel, A., 2001. Paleoproterozoic framework of the Guiana Shield II-continental scale boudinage and ultra-high temperature granulite belt production at 2.07-2.06 Ga.
- Delor, C., Lahondère, D., Egal, E., Lafon, J. M., Cocherie, A., Guerrot, C., Rossi, P., Truffert, C., Théveniaut, H., Phillips, D. & de Avelar, V. G., 2003. Transamazonian crustal growth and reworking as revealed by the 1: 500,000-scale geological map of French Guiana, Géologie de la France.
- Dewey, J. F., Holdsworth, R. E. & Strachan, R. A., 1998. Transpression and transtension zones. *Geological Society, London, Special Publications*, **135**(1), 1-14.
- Dhuime, B., Hawkesworth, C. J., Cawood, P. A. & Storey, C. D., 2012. A change in the geodynamics of continental growth 3 billion years ago. *Science*, **335**(6074), 1334-1336.
- Dickson, B. & Scott, K., 1997. Interpretation of aerial gamma-ray surveys-adding the geochemical factors. *AGSO Journal of Australian Geology and Geophysics*, **17**, 187-200.

- Diener, J., Stevens, G. & Kisters, A., 2013. High-Pressure Intermediate-Temperature Metamorphism in the Southern Barberton Granitoid–Greenstone Terrain, South Africa: A Consequence of Subduction-Driven Overthickening and Collapse of Mid-Archean Continental Crust. In: *Archean Geodynamics and Environments*, pp. 239-254, American Geophysical Union.
- Doumbia, S., Pouclet, A., Kouamelan, A., Peucat, J. J., Vidal, M. & Delor, C., 1998. Petrogenesis of juvenile-type Birimian (Paleoproterozoic) granitoids in Central Côte-d'Ivoire, West Africa: geochemistry and geochronology. *Precambrian Research*, **87**, 33-63.
- Duchene, S., Aissa, R. & Vanderhaeghe, O., 2006. Pressure-temperature-time evolution of metamorphic rocks from Naxos (Cyclades, Greece): Constraints from thermobarometry and Rb/Sr dating. *Geodinamica Acta*, **19**(5), 301-321.
- Duclaux, G., Rey, P., Guillot, S. & Ménot, R.-P., 2007. Orogen-parallel flow during continental convergence: Numerical experiments and Archean field examples. *Geology*, **35**(8), 715-718.
- Egal, E., Thiéblemont, D., Lahondère, D., Guerrot, C., Costea, C. A., Iliescu, D., Delor, C., Goujou, J.-C., Lafon, J. M., Tegye, M., Diaby, S. & Kolié, P., 2002. Late Eburnean granitization and tectonics along the western and northwestern margin of the Archean Kénéma–Man domain (Guinea, West African Craton). *Precambrian Research*, **117**(1–2), 57-84.
- Eisenlohr, B. N., 1989. *The structural geology of Birimian and Tarkwaian rocks of southwest Ghana*. BGR, Hannover.
- Eisenlohr, B. N. & Hirdes, W., 1992. The structural development of the early Proterozoic Birimian and tarkwaian rocks of southwest Ghana, West Africa. *Journal of African Earth Sciences (and the Middle East)*, **14**(3), 313-325.
- England, P. C. & Thompson, A. B., 1984. Pressure—temperature—time paths of regional metamorphism I. Heat transfer during the evolution of regions of thickened continental crust. *Journal of Petrology*, **25**(4), 894-928.
- Ernst, W., 2005. Alpine and Pacific styles of Phanerozoic mountain building: subduction - zone petrogenesis of continental crust. *Terra Nova*, **17**(2), 165-188.
- Ernst, W. G., 2009. Archean plate tectonics, rise of Proterozoic supercontinentality and onset of regional, episodic stagnant-lid behavior. *Gondwana Research*, **15**(3–4), 243-253.
- Fabre, R., Ledru, P. & Milesi, J.-P., 1990. Le Protérozoïque inférieur (Birimien) du centre de la Côte-d'Ivoire: évolution tectonique et corrélations. *Comptes rendus de l'Académie des sciences. Série 2, Mécanique, Physique, Chimie, Sciences de l'univers, Sciences de la Terre*, **311**(8), 971-976.
- Feybesse, J.-L., Billa, M., Guerrot, C., Duguey, E., Lescuyer, J.-L., Milési, J.-P. & Bouchot, V., 2006. The Paleoproterozoic Ghanaian province: Geodynamic model and ore controls, including regional stress modeling. *Precambrian Research*, **149**(3 - 4), 149-196.
- Fischer, R. & Gerya, T., 2016. Regimes of subduction and lithospheric dynamics in the Precambrian: 3D thermomechanical modelling. *Gondwana Research*, **37**, 53-70.
- Fossen, H., Cavalcante, G. C. G., Pinheiro, R. V. L. & Archanjo, C. J., 2018. Deformation–Progressive or multiphase? *Journal of Structural Geology*.
- Fossen, H., Teyssier, C. & Whitney, D. L., 2013. Transtensional folding. *Journal of Structural Geology*, **56**, 89-102.
- François, C., Philippot, P., Rey, P. & Rubatto, D., 2014. Burial and exhumation during Archean sagduction in the East Pilbara granite-greenstone terrane. *Earth and Planetary Science Letters*, **396**, 235-251.
- Galipp, K., Klemd, R. & Hirdes, W., 2003. Metamorphism and geochemistry of the Palaeoproterozoic Birimian Sefwi volcanic belt (Ghana, West Africa). *Geologisches Jahrbuch D 111*, 151 - 191.
- Ganne, J., De Andrade, V., Weinburg, R. F., Vidal, O., Dubacq, B., Kagambega, N., Naba, S., Baratoux, L., Jessell, M. W. & Allibone, J., 2012. Modern-style plate subduction preserved in the Palaeoproterozoic West Africa craton. *Nature Geoscience Letters*, **5**, 60 - 65.
- Ganne, J. & Feng, X., 2017. Primary magmas and mantle temperatures through time. *Geochemistry, Geophysics, Geosystems*, **18**(3), 872-888.
- Ganne, J., Gerbault, M. & Block, S., 2014. Thermo-mechanical modeling of lower crust exhumation—Constraints from the metamorphic record of the Palaeoproterozoic Eburnean orogeny, West African Craton. *Precambrian Research*, **243**, 88-109.
- Gasquet, D., Barbey, P., Adou, M. & Paquette, J. L., 2003. Structure, Sr–Nd isotope geochemistry and zircon U–Pb geochronology of the granitoids of the Dabakala area (Côte d'Ivoire): evidence for a 2.3 Ga

- crustal growth event in the Palaeoproterozoic of West Africa? *Precambrian Research*, **127**(4), 329-354.
- Gerya, T., 2014. Precambrian geodynamics: concepts and models. *Gondwana Research*, **25**(2), 442-463.
- Gueye, M., Ngom, P. M., Diène, M., Thiam, Y., Siegesmund, S., Wemmer, K. & Pawlig, S., 2008. Intrusive rocks and tectono-metamorphic evolution of the Mako Paleoproterozoic belt (Eastern Senegal, West Africa). *Journal of African Earth Sciences*, **50**(2-4), 88-110.
- Gunn, P. J., Maidment, D. & Milligan, P., 1995. Interpreting aeromagnetic data in areas of limited outcrop: an example from the Arunta Block, Northern Territory. *Exploration Geophysics*, **26**(3), 227-232.
- Harley, S., 1992. Proterozoic granulite terranes. *Developments in Precambrian Geology*, **10**, 301-359.
- Harley, S. L. & Motoyoshi, Y., 2000. Al zoning in orthopyroxene in a sapphirine quartzite: evidence for > 1120 C UHT metamorphism in the Napier Complex, Antarctica, and implications for the entropy of sapphirine. *Contributions to Mineralogy and Petrology*, **138**(4), 293-307.
- Hein, K. A. A., 2010. Succession of structural events in the Goren greenstone belt (Burkina Faso): Implications for West African tectonics. *Journal of African Earth Sciences*, **56**(2-3), 83-94.
- Herzberg, C., Condie, K. & Korenaga, J., 2010. Thermal history of the Earth and its petrological expression. *Earth and Planetary Science Letters*, **292**(1), 79-88.
- Hirdes, W. & Davis, D. W., 1998. First U–Pb zircon age of extrusive volcanism in the Birimian Supergroup of Ghana/West Africa. *Journal of African Earth Sciences*, **27**(2), 291-294.
- Hirdes, W. & Davis, D. W., 2002. U–Pb Geochronology of Paleoproterozoic Rocks in the Southern Part of the Kedougou-Kéniéba Inlier, Senegal, West Africa: Evidence for Diachronous Accretionary Development of the Eburnean Province. *Precambrian Research*, **118**(1-2), 83-99.
- Hirdes, W., Davis, D. W. & Eisenlohr, B. N., 1992. Reassessment of Proterozoic granitoid ages in Ghana on the basis of U/Pb zircon and monazite dating. *Precambrian Research*, **56**(1–2), 89-96.
- Hirdes, W., Davis, D. W., Lüdtke, G. & Konan, G., 1996. Two generations of Birimian (Paleoproterozoic) volcanic belts in northeastern Côte d'Ivoire (West Africa): consequences for the 'Birimian controversy'. *Precambrian Research*, **80**(3-4), 173-191.
- Hirdes, W., Konan, G., N'da, D., Okou, A., Sea, P. & Zamble, Z., 2003. Carte géologique de Cote d'Ivoire 1:100 000, feuille Aboisso. , Direction de la Géologie, Ministère des Mines et de l'Energie, Abidjan, Cote d'Ivoire.
- Hirdes, W., Konan, K. G., N'Da, D., Okou, A., Sea, P., Zamble, Z. B. & Davis, D. W., 2007. *Geology of the Northern Portion of the Oboisso Area, Côte d'Ivoire. Sheets 4A, 4B, 4B BIS, 4D.* Direction de la Géologie, Abidjan, Côte d'Ivoire and Bundesanstalt für Geowissenschaften und Rohstoffe, Hanover.
- Hirdes, W. & Nunoo, B., 1994. The Proterozoic paleoplacers at Tarkwa gold mine, SW Ghana: sedimentology, mineralogy, and precise age dating of the Main Reef and West Reef, and bearing of the investigations on source area aspects. *Geologisches Jahrbuch D*, **100**, 247-311.
- Hirdes, W., Senger, R., Adjei, J., Efa, E., Loh, G. K. & Tettey, A., 1993. *Explanatory notes for the geological map of southwest Ghana 1:100 000.* Bundesanstalt für Geowissenschaften und Rohstoffe, Hannover.
- Hurley, P., Rand, J., Pinson, W., Fairbairn, H., de Almeida, F., Melcher, G., Cordani, U., Kawashita, K. & Vandroos, P., 1967. Test of continental drift by comparison of radiometric ages. *Science*, **157**(3788), 495-500.
- Jessell, M., Santoul, J., Baratoux, L., Youbi, N., Ernst, R. E., Metelka, V., Miller, J. & Perrouy, S., 2015. An updated map of West African mafic dykes. *Journal of African Earth Sciences*, **112**, 440-450.
- Jessell, M. W., Amponsah, P. O., Baratoux, L., Asiedu, D. K., Loh, G. K. & Ganne, J., 2012. Crustal-scale transcurrent shearing in the Paleoproterozoic Sefwi-Sunyani-Comoé region, West Africa. *Precambrian Research*, **212–213**(0), 155-168.
- John, T., Klemd, R., Hirdes, W. & Loh, G., 1999. The metamorphic evolution of the Paleoproterozoic (Birimian) volcanic Ashanti belt (Ghana, West Africa). *Precambrian Research*, **98**, 11-30.
- Junner, N. R., 1940. Geology of the Gold Coast and Western Togoland. *Gold Coast Geol. Surv. Bull.*, **11**(11), 1–40.
- Junner, N. R., 1946. Geology and hydrology of the Voltaian basin.
- Kalsbeek, F., Frei, D. & Affaton, P., 2008. Constraints on provenance, stratigraphic correlation and structural context of the Volta basin, Ghana, from detrital zircon geochronology: An Amazonian connection? *Sedimentary Geology*, **212**(1–4), 86-95.
- Keller, C. B. & Schoene, B., 2012. Statistical geochemistry reveals disruption in secular lithospheric evolution about 2.5 Gyr ago. *Nature*, **485**(7399), 490.



- Kelsey, D., Clark, C. & Hand, M., 2008. Thermobarometric modelling of zircon and monazite growth in melt-bearing systems: Examples using model metapelitic and metapsammitic granulites. *Journal of Metamorphic Geology*, **26**(2), 199-212.
- Kiessling, R., 1997. Sedimentation and structure in the Tarkwaian Group of the Bui Basin in West-Ghana. In: *Geological, geophysical and geochemical investigations in the Bui belt area in Ghana* (ed Zitzmann, A.), pp. 113-182, Geologische Jahrbuch, Reihe B.
- Klein, E. L., Moura, C. A. & Pinheiro, B. L., 2005. Paleoproterozoic crustal evolution of the São Luís Craton, Brazil: evidence from zircon geochronology and Sm-Nd isotopes. *Gondwana Research*, **8**(2), 177-186.
- Klein, E. L. & Moura, C. A. V., 2008. São Luís craton and Gurupi Belt (Brazil): possible links with the West African craton and surrounding Pan-African belts. *Geological Society, London, Special Publications*, **294**(1), 137-151.
- Komiya, T., Hayashi, M., Maruyama, S. & Yurimoto, H., 2002. Intermediate-P/T type Archean metamorphism of the Isua supracrustal belt: Implications for secular change of geothermal gradients at subduction zones and for Archean plate tectonics. *American Journal of Science*, **302**(9), 806-826.
- Korenaga, J., 2013. Archean Geodynamics and the Thermal Evolution of Earth. In: *Archean Geodynamics and Environments*, pp. 7-32, American Geophysical Union.
- Kouamelan, A. N., Delor, C. & Peucat, J.-J., 1997. Geochronological evidence for reworking of Archean terrains during the early Proterozoic (2.1 Ga) in the western Cote d'Ivoire (Man Rise-West African Craton). *Precambrian Research*, **86**(3), 177-199.
- Krabbendam, M. & Dewey, J. F., 1998. Exhumation of UHP rocks by transtension in the Western Gneiss Region, Scandinavian Caledonides. *Geological Society, London, Special Publications*, **135**(1), 159-181.
- Kříbek, B., Sýkorová, I., Machovič, V. & Laufek, F., 2008. Graphitization of organic matter and fluid-deposited graphite in Palaeoproterozoic (Birimian) black shales of the Kaya - Goren greenstone belt (Burkina Faso, West Africa). *Journal of Metamorphic Geology*, **26**(9), 937-958.
- Kroonenberg, S., De Roever, E., Fraga, L., Reis, N., Faraco, T., Lafon, J.-M., Cordani, U. & Wong, T. E., 2016. Paleoproterozoic evolution of the Guiana Shield in Suriname: A revised model. *Netherlands Journal of Geosciences*, **95**(4), 491-522.
- Lemoine, S., Tempier, P., Bassot, J., Caen - Vachette, M., Vialette, Y., Toure, S. & Wenmenga, U., 1990. The Burkinian orogenic cycle, precursor of the Eburnian orogeny in West Africa. *Geological Journal*, **25**(2), 171-188.
- Leube, A., Hirdes, W., Mauer, R. & Kesse, G. O., 1990. The early Proterozoic Birimian Supergroup of Ghana and some aspects of its associated gold mineralization. *Precambrian Research*, **46**(1-2), 139-165.
- Li, X., 2008. Magnetic reduction-to-the-pole at low latitudes: Observations and considerations. *The leading edge*, **27**(8), 990-1002.
- Liégeois, J. P., Claessens, W., Camara, D. & Klerkx, J., 1991. Short-lived Eburnian orogeny in southern Mali. Geology, tectonics, U-Pb and Rb-Sr geochronology. *Precambrian Research*, **50**(1-2), 111-136.
- Lindsay, M. D., Perrouy, S., Jessell, M., Aillères, L., De Kemp, E. & Betts, P. G., 2011. Categorising features of geological terranes with geodiversity metrics: Enhancing exploration of multiple geological models, pp. 648-654.
- Loh, G., Hirdes, W., Anani, C., Davis, D. W. & Vetter, U. K., 1999. Explanatory Notes for the Geological Map of-Southwest Ghana 1: 100,000-Sekondi (0402A) and Axim (0403B) Sheets. In: *Geologisches Jahrbuch Reihe B Heft 93*, BGR, Hannover.
- Lompo, M., 2009. Geodynamic evolution of the 2.25-2.0 Ga Palaeoproterozoic magmatic rocks in the Man-Leo shield of the West African Craton. A model of subsidence of an oceanic plateau. In: *Palaeoproterozoic Supercontinents and Global Evolution*, pp. 231-254, Geological Society, London.
- Lompo, M., 2010. Paleoproterozoic structural evolution of the Man-Leo Shield (West Africa). Key structures for vertical to transcurrent tectonics. *Journal of African Earth Sciences*, **58**, 19 - 36.
- Lüdtke, G., Hirdes, W., Konan, G., Kone, Y., N'da, D., Traore, Y. & Zamble, B. Z., 1999. Géologie de la région Haute Comoé Sud - feuilles Dabakala (2b, d et 4b, d), Direction de la Géologie, Abidjan.
- Luo, Y., Xue, D.-J. & Wang, M., 2010. reduction to the pole at the geomagnetic equator. *Chinese Journal of Geophysics* **53**(6), 1082-1089.
- MacLeod, I. N., Jones, K. & Dai, T. F., 1993. 3-D analytic signal in the interpretation of total magnetic field data at low magnetic latitudes. *Exploration Geophysics*, **24**(4), 679-688.

- McFarlane, H. B., 2018. *The geodynamic and tectonic evolution of the Palaeoproterozoic Sefwi Greenstone Belt, West African Craton (Ph.D. Manuscript)*, Monash University.
- Metelka, V., Baratoux, L., Naba, S. & Jessell, M. W., 2011. A geophysically constrained litho-structural analysis of the Eburnean greenstone belts and associated granitoid domains, Burkina Faso, West Africa. *Precambrian Research*, **190**(1–4), 48-69.
- Milési, J., Feybesse, J., Ledru, P., Dommanget, A., Ouedraogo, M., Marcoux, E., Prost, A., Vinchon, C., Sylvain, J. & Johan, V., 1989. West African gold deposits in their Lower Proterozoic lithostructural setting. *Chron. rech. min.*, **497**(3), 98.
- Milési, J. P., Ledru, P., Feybesse, J.-L., Dommanget, A. & Marcoux, E., 1992. Early Proterozoic ore deposits and tectonics of the Birimian orogenic belt, West Africa. *Precambrian Research*, **58**, 305 - 344.
- Milligan, P. R. & Gunn, P. J., 1997. Enhancement and presentation of airborne geophysical data. *AGSO Journal of Australian Geology and Geophysics*, **17**(2), 63-75.
- Minty, B., Luyendyk, A. & Brodie, R., 1997. Calibration and data processing for airborne gamma-ray spectrometry. *AGSO Journal of Australian Geology and Geophysics*, **17**, 51-62.
- Moyen, J.-F., Stevens, G. & Kisters, A., 2006. Record of mid-Archaean subduction from metamorphism in the Barberton terrain, South Africa. *Nature*, **442**(7102), 559-562.
- Mueller, W. U., Daigneault, R., Mortensen, J. K. & Chown, E. H., 1996. Archean terrane docking: upper crust collision tectonics, Abitibi greenstone belt, Quebec, Canada. *Tectonophysics*, **265**(1), 127-150.
- Mumin, A. H. & Fleet, M., 1995. Evolution of gold mineralization in the Ashanti Gold Belt, Ghana: evidence from carbonate compositions and parageneses. *Mineralogy and Petrology*, **55**(4), 265-280.
- O'Neill, C., Lenardic, A., Moresi, L., Torsvik, T. & Lee, C.-T., 2007. Episodic precambrian subduction. *Earth and Planetary Science Letters*, **262**(3), 552-562.
- Oberthür, T., Vetter, U., Davis, D. W. & Amanor, J. A., 1998. Age constraints on gold mineralization and Paleoproterozoic crustal evolution in the Ashanti belt of southern Ghana. *Precambrian Research*, **89**(3-4), 129-143.
- Opere-Addo, E., Browning, P. & John, B. E., 1993. Pressure-temperature constraints on the evolution of an Early proterozoic plutonic suite in southern Ghana, West Africa. *Journal of African Earth Sciences (and the Middle East)*, **17**(1), 13-22.
- Ouzegane, K., Kienast, J.-R., Bendaoud, A. & Drareni, A., 2003. A review of Archaean and Paleoproterozoic evolution of the In Ouzzal granulitic terrane (Western Hoggar, Algeria). *Journal of African Earth Sciences*, **37**(3-4), 207-227.
- Parra-Avila, L., 2015. 4D Evolution of the Paleoproterozoic Baoulé-Mossi Domain of the West African Craton. *Unpublished Ph. D thesis. University of Western Australia*, 527.
- Parra-Avila, L. A., Belousova, E., Fiorentini, M. L., Baratoux, L., Davis, J., Miller, J. & McCuaig, T. C., 2016. Crustal evolution of the Paleoproterozoic Birimian terranes of the Baoulé-Mossi domain, southern West African Craton: U–Pb and Hf-isotope studies of detrital zircons. *Precambrian Research*, **274**, 25-60.
- Parra-Avila, L. A., Kemp, A. I. S., Fiorentini, M. L., Belousova, E., Baratoux, L., Block, S., Jessell, M., Bruguier, O., Begg, G. C., Miller, J., Davis, J. & McCuaig, T. C., 2017. The geochronological evolution of the Paleoproterozoic Baoulé-Mossi domain of the Southern West African Craton. *Precambrian Research*, **300**, 1-27.
- Pattison, D., 2003. Petrogenetic significance of orthopyroxene - free garnet+ clinopyroxene+ plagioclase ± quartz - bearing metabasites with respect to the amphibolite and granulite facies. *Journal of Metamorphic Geology*, **21**(1), 21-34.
- Pawlig, S., Gueye, M., Klischies, R., Schwarz, S., Wemmer, K. & Siegesmund, S., 2006. Geochemical and Sr-Nd isotopic data on the Birimian of the Kedougou-Kenieba inlier (Eastern Senegal): Implications on the Palaeoproterozoic evolution of the West African craton. *South African Journal of Geology*, **109**(3), 411-427.
- Perrouy, S., Aillères, L., Jessell, M. W., Baratoux, L., Bourassa, Y. & Crawford, B., 2012. Revised Eburnean geodynamic evolution of the gold-rich southern Ashanti Belt, Ghana, with new field and geophysical evidence of pre-Tarkwaian deformations. *Precambrian Research*, **204–205**, 12-39.
- Petersson, A., Scherstén, A., Kemp, A., Kristinsdóttir, B., Kalvig, P. & Anum, S., 2016. Zircon U-Pb-Hf evidence for subduction related crustal growth and reworking of Archaean crust within the Palaeoproterozoic Birimian terrane, West African Craton, SE Ghana. *Precambrian Research*, **275**, 286-309.

- Pigois, J. P., Groves, D. I., Fletcher, I. R., McNaughton, N. J. & Snee, L. W., 2003. Age constraints on Tarkwaian palaeoplacer and lode-gold formation in the Tarkwa-Damang district, SW Ghana. *Mineralium Deposita*, **38**(6), 695-714.
- Pilkington, M. & Keating, P., 2009. The utility of potential field enhancements for remote predictive mapping. *Canadian Journal of Remote Sensing*, **35**(S1), S1-S11.
- Pitra, P., Kouamelan, A. N., Ballèvre, M. & Peucat, J. J., 2010. Palaeoproterozoic high-pressure granulite overprint of the Archean continental crust: evidence for homogeneous crustal thickening (Man Rise, Ivory Coast). *Journal of Metamorphic Geology*, **28**(1), 41-58.
- Polat, A. & Kerrich, R., 1999. Formation of an Archean tectonic mélange in the Schreiber - Hemlo greenstone belt, Superior Province, Canada: Implications for Archean subduction - accretion process. *Tectonics*, **18**(5), 733-755.
- Pons, J., Barbey, P., Dupuis, D. & Léger, J. M., 1995. Mechanisms of pluton emplacement and structural evolution of a 2.1 Ga juvenile continental crust: the Birimian of southwestern Niger. *Precambrian Research*, **70**(3-4), 281-301.
- Pouclot, A., Doumbia, S. & Vidal, M., 2006. Geodynamic setting of the Birimian volcanism in central Ivory Coast (western Africa) and its place in the Palaeoproterozoic evolution of the Man Shield. *Bulletin de la Société Géologique de France*, **177**(2), 105-121.
- Pouclot, A., Vidal, M., Delor, C., Simeon, Y. & Alric, G., 1996. Le volcanisme birimien du nord-est de la Côte-d'Ivoire, mise en évidence de deux phases volcano-tectoniques distinctes dans l'évolution géodynamique du Paléoproterozoïque. *Bulletin de la Société géologique de France*, **167**(4), 529-541.
- Rey, P. F. & Houseman, G., 2006. Lithospheric scale gravitational flow: the impact of body forces on orogenic processes from Archaean to Phanerozoic. *Geological Society, London, Special Publications*, **253**(1), 153-167.
- Rey, P. F., Mondy, L., Duclaux, G., Teyssier, C., Whitney, D. L., Bocher, M. & Prigent, C., 2017. The origin of contractional structures in extensional gneiss domes. *Geology*, **45**(3), 263-266.
- Rocci, G., 1965. Essai d'interprétation de mesures géochronologiques. La structure de l'Ouest africain. *Sciences Terre Nancy*, **10**, 461-479.
- Royden, L. H., Burchfiel, B. C. & van der Hilst, R. D., 2008. The geological evolution of the Tibetan Plateau. *science*, **321**(5892), 1054-1058.
- Sizova, E., Gerya, T. & Brown, M., 2014. Contrasting styles of Phanerozoic and Precambrian continental collision. *Gondwana Research*, **25**(2), 522-545.
- Sizova, E., Gerya, T., Brown, M. & Perchuk, L., 2010. Subduction styles in the Precambrian: insight from numerical experiments. *Lithos*, **116**(3), 209-229.
- Stern, R. J., 2005. Evidence from ophiolites, blueschists, and ultrahigh-pressure metamorphic terranes that the modern episode of subduction tectonics began in Neoproterozoic time. *Geology*, **33**(7), 557-560.
- Stern, R. J., 2007. When and how did plate tectonics begin? Theoretical and empirical considerations. *Chinese Science Bulletin*, **52**(5), 578-591.
- Stewart, J. R., Betts, P. G., Collins, A. S. & Schaefer, B. F., 2009. Multi-scale analysis of Proterozoic shear zones: An integrated structural and geophysical study. *Journal of Structural Geology*, **31**(10), 1238-1254.
- Sullivan, W. A., 2013. L tectonites. *Journal of Structural Geology*, **50**, 161-175.
- Tapsoba, B., Lo, C.-H., Jahn, B.-M., Chung, S.-L., Wenmenga, U. & Iizuka, Y., 2013. Chemical and Sr-Nd isotopic compositions and zircon U-Pb ages of the Birimian granitoids from NE Burkina Faso, West African Craton: Implications on the geodynamic setting and crustal evolution. *Precambrian Research*, **224**, 364-396.
- Thébaud, N. & Rey, P. F., 2013. Archean gravity-driven tectonics on hot and flooded continents: Controls on long-lived mineralised hydrothermal systems away from continental margins. *Precambrian Research*, **229**(Supplement C), 93-104.
- Torquato, J. R. & Cordani, U. G., 1981. Brazil-Africa geological links. *Earth-Science Reviews*, **17**(1), 155-176.
- Triboulet, C. & Feybesse, J.-L., 1998. Les métabasites birimiennes et archéennes de la région de Toulepleu-Iti (Côte-d'Ivoire): des roches portées à 8 kbar ( $\approx$  24 km) et 14 kbar ( $\approx$  42 km) au Paléoproterozoïque. *Comptes Rendus de l'Académie des Sciences-Series IIA-Earth and Planetary Science*, **327**(1), 61-66.

- Tshibubudze, A., Hein, K., Peters, L., Woolfe, A. & McCUAIG, T., 2013. Oldest U-Pb crystallization age for the West African Craton from the Oudalan-Gorouol Belt of Burkina Faso. *South African Journal of Geology*, **116**(1), 169-181.
- Tunks, A. J., Selley, D., Rogers, J. R. & Brabham, G., 2004. Vein mineralization at the Damang Gold Mine, Ghana: controls on mineralization. *Journal of Structural Geology*, **26**(6-7), 1257-1273.
- Väisänen, M. & Hölttä, P., 1999. Structural and metamorphic evolution of the Turku migmatite complex, southwestern Finland. *Bulletin of the Geological Society of Finland*, **71**(1), 177-218.
- Van der Hilst, R., Widiyantoro, S. & Engdahl, E., 1997. Evidence for deep mantle circulation from global tomography. *Nature*, **386**(6625), 578.
- van Hunen, J. & Moyon, J.-F., 2012. Archean subduction: fact or fiction? *Annual Review of Earth and Planetary Sciences*, **40**, 195-219.
- van Hunen, J. & van den Berg, A. P., 2008. Plate tectonics on the early Earth: limitations imposed by strength and buoyancy of subducted lithosphere. *Lithos*, **103**(1), 217-235.
- Van Kranendonk, M. J., Hugh Smithies, R., Hickman, A. H. & Champion, D. C., 2007. Review: secular tectonic evolution of Archean continental crust: interplay between horizontal and vertical processes in the formation of the Pilbara Craton, Australia. *Terra Nova*, **19**(1), 1-38.
- van Staal, C. R., Whalen, J. B., Valverde-Vaquero, P., Zagorevski, A. & Rogers, N., 2009. Pre-Carboniferous, episodic accretion-related, orogenesis along the Laurentian margin of the northern Appalachians. *Geological Society, London, Special Publications*, **327**(1), 271-316.
- Vanderhaeghe, O., Ledru, P., Thiéblemont, D., Egal, E., Cocherie, A., Tegye, M. & Milési, J.-P., 1998. Contrasting mechanism of crustal growth: geodynamic evolution of the Paleoproterozoic granite-greenstone belts of French Guiana. *Precambrian Research*, **92**(2), 165-193.
- Vanderhaeghe, O. & Teyssier, C., 2001. Partial melting and flow of orogens. *Tectonophysics*, **342**(3), 451-472.
- Verduzco, B., Fairhead, J. D., Green, C. M. & MacKenzie, C., 2004. New insights into magnetic derivatives for structural mapping. *The Leading Edge*, **23**(2), 116-119.
- Vidal, M. & Alric, G., 1994. The palaeoproterozoic (Birimian) of Haute-Comoé in the West African craton, Ivory Coast: a transtensional back-arc basin. *Precambrian Research*, **65**(1-4), 207-229.
- Vidal, M., Gumiaux, C., Cagnard, F., Pouclet, A., Ouattara, G. & Pichon, M., 2009. Evolution of a Paleoproterozoic "weak type" orogeny in the West African Craton (Ivory Coast). *Tectonophysics*, **477**(3-4), 145-159.
- Wilford, J., Bierworth, P. N. & Craig, M. A., 1997. Application of airborne gamma-ray spectrometry in soil/regolith mapping. *AGSO Journal of Australian Geology and Geophysics*, **17**, 201-216.
- Windley, B. F., Alexeev, D., Xiao, W., Kröner, A. & Badarch, G., 2007. Tectonic models for accretion of the Central Asian Orogenic Belt. *Journal of the Geological Society*, **164**(1), 31-47.
- Zitzmann, A., Keissling, R. & Loh, G. K., 1997. Geology in the Bui belt area in Ghana. In: *Geological, Geophysical and Geochemical investigations in the Bui belt area in Ghana* (ed Zitzmann, A.), pp. 7-112, Geologische Jahrbuch, Reihe B.

## 11. Supplementary data I – VI

Fig. 1SI. Composite image of greyscale reduced to the pole (RTP) of the residual magnetic intensity and associated individual survey details.

Table 1SI. Geophysical survey acquisition details.

Fig. 2SI. Bouguer gravity anomaly grid of survey area

Fig. 3SI. Composite image of negative reduced to the equator (RTE) of the residual magnetic intensity (RMI) with greyscale first vertical derivative (1VD) for all surveys utilized in the study

Fig. 4SI. Greyscale digital elevation model of study area with ternary image of gamma-ray signal from three channels, K, eTh, and eU, highlighting the partial coverage of radiometric data of the study area

Fig. 5SI. Measured magnetic susceptibility values for individual lithologies presented in histograms to display range and frequency.

Fig. 6SI. Field photos of individual lithologies.

*Table 1. Synthesis of the mineralogy, petrophysical properties and geophysical signatures of the lithologies represented on the geological map (Fig. 2). Thumbnails represent subsets of geophysical datasets, using the same methodology as described in section 4. Scale bar is 4km in length.*

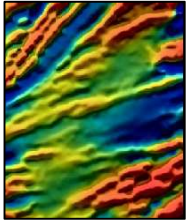
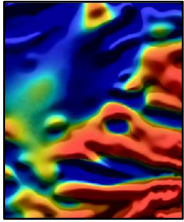
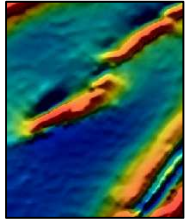
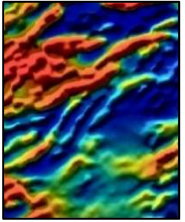
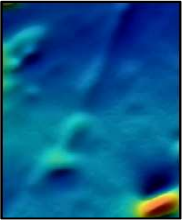
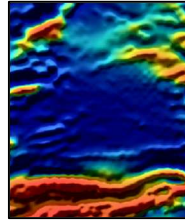
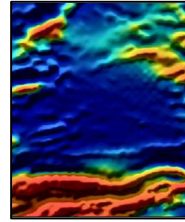
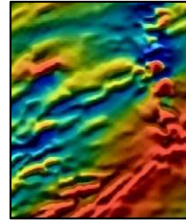
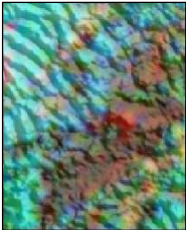
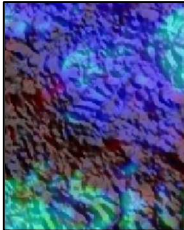

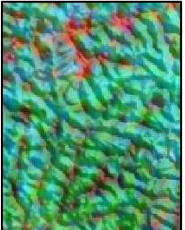
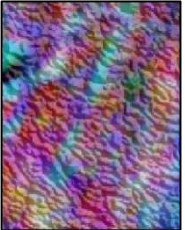


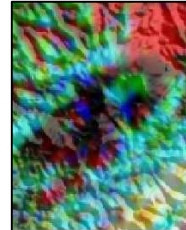
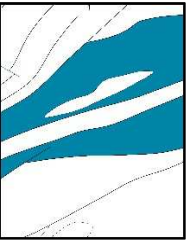

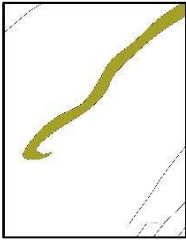

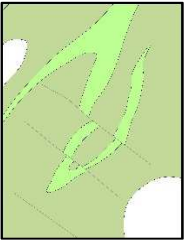
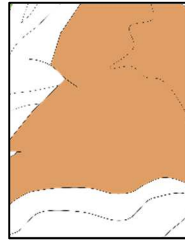
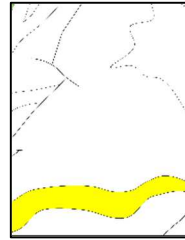
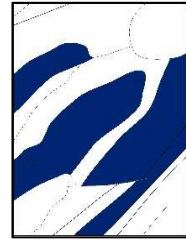
Lithology	Basalt/metabasalt/ metadolerite	Meta- andesite/dacite	Rhyolite/felsic volcaniclastite	Volcaniclastic metasediments	Volcano- sedimentary schist	Composite gneiss	Mafic orthogneiss	Gabbro/norite/pyroxenite complex
Mineralogy	Hbl, qz, (relict Cpx), bt, pl, chl, act, ep, cal	pl, hbl, qz, ep, ttn, chl, act	qz, chl, wm,	Qz, pl, chl, wm, ± bt, hbl, grt	qz, chl, ms, gr	qz, bt, pl, wm, grt, ± alsi, tur, gr	pl, hbl, qz, ilm, grt, ep, ttn	hbl (after cpx), pl, chl, ep, act
Magnetic susceptibility range (10 <sup>-3</sup> SI)	0.05, 1.01–9.58, 13.08–84.00 (multimodal)	0.03–0.40, 7.41– 39.50 (bimodal)	0.02–1.60, 6.25– 29.14 (bimodal)	0.06–1.00, 20.01– 80.30 (bimodal)	0.02–1.30	0.04–1.30	0.12–9.58 (bimodal)	0.27–2.48
Sample	SB040	SB173	SB044	SB439	SB362	SB398	SB177	SB411
U (ppm)	0.90	1.70	1.50	1.60	1.40	1.50	0.40	0.80
Th (ppm)	1.80	4.60	6.30	3.70	4.10	4.60	0.20	1.60
K <sub>2</sub> O (wt%)	1.17	1.54	2.3	2.63	2.79	3.16	0.2	0.81
Airborne magnetic response	Highly magnetic, heterogeneous, elongate near SZ	Low to high intensity	Low to very highly magnetic layers	Low to high, heterog. strong magnetic fabric	Low intensity, uniform, smooth	Very low to low intensity, smooth	Low to high intensity, variable magnetic fabric	Low to moderate intensity, weak magnetic fabric
Magnetic image								
Airborne radiometric response	U, Th, K poor (dark), pervasive K alteration along SZ	Enriched in U relative to Th and K	Low U, moderate Th, high K (red - orange)	Low U, K, moderate Th, regolith (light blue)	Low U, Th, mod K, higher K in Kumasi domain (pink - red)	Moderate to high U, Th, K (pink- yellow)	Heterogeneous signal often covered by regolith	U, Th, K poor (dark)
Radiometric + shaded DEM								
Map								

Table 1 continued.

Lithology	G1: Trondhjemite, tonalite, granodiorite	G2: Trondhjemite and granodiorite	G3a: Granodiorite, quartz diorite	G3b: Potassic quartz monzonite	G4: Leucogranite	Chemical sediment (Chert)	Polymictic conglomerate	Dolerite dyke
Mineralogy	qz, pl, bt, hbl, ± kfs	qz, pl, bt, hbl, ± kfs, ep	pl, kfs, qz, hbl, bt	qz, kfs, pl, bt (± hbl)	qz, kfs, pl, bt, ms	No data	qz, pl, chl, wm, ep, py	ol, opx, cpx, pl, hbl, bt
Magnetic susceptibility range ( $10^{-3}$ SI)	0.15–0.55, 1.01–3.50, 15.47–25.30 (multimodal)	0.12–2.03	0.09–1.00, 4.25–24.04 (bimodal)	0.47–3.88	0.00–0.15	0.35–1.59	0.01–0.50	0.08–0.16, 10.55–87.70 (bimodal)
Sample	SB252	SB248	SB045	SB023	SB010	SB171	SB417	SB431
U (ppm)	1.90	0.50	2.00	0.60	7.20	no data	no data	0.89
Th (ppm)	4.70	1.50	5.70	0.50	4.20			2.91
K <sub>2</sub> O (wt%)	1.84	1.24	1.82	4.01	2.51			1.13
Airborne magnetic response	Low to moderate intensity, strong magnetic fabric	Low to moderate, homogeneous, smooth	Moderate magnetic intensity, weak magnetic fabric	Moderate to high, moderate strength magnetic fabric	Low, homogeneous	Variable low to moderate intensity	Narrow, low intensity signal	Strong, linear signal
Magnetic image								
Airborne radiometric response	K, Th, U poor (dark) heterogeneous	Heterog. relative enrichment in Th, U, K, Th, poor (dark)	Low K, high Th, low U (green)	High K, mod U, low Th (red - pink)	High K, moderate Th, U,	Depleted in U, Th and K (dark)	High in K, U, Th (white) and rich in K close to SZ	Diapole effect, No clear signal
Radiometric + shaded DEM								
Map								